Available online at www.sciencedirect.com
SCIENCE DIRECT®
Ecological Modelling 193 (2006) 141–181
ECOLOGICAL MODELLING
www.elsevier.com/locate/ecolmodel

A holistic tree seedling model for the investigation of functional trait diversity

Christian O. Marks *, Martin J. Lechowicz

Department of Biology, McGill University, 1205 Docteur Penfield Avenue, Montréal, Que., Canada H3A 1B1

Received 24 February 2005; received in revised form 11 September 2005; accepted 25 September 2005
Available online 16 November 2005

Abstract

Improved insights into the basis for the large variation in plant traits observed in nature are expected from the development of more holistic optimization models. Holistic approaches emphasize the effects of interactions and tradeoffs among multiple traits on whole plant fitness rather than studying individual traits in isolation. Using this holistic approach, we developed a general model of tree seedling form and function. Here we present this new model and examine its realism and utility. The modeled growth of tree seedlings reproduced natural patterns accurately, including subtle ontogenetic shifts and environmental responses. The underlying processes of resource acquisition also behaved realistically, including the key process of stomatal control. Due to its holistic approach and the generality of the tradeoffs on which it is based, the model is well suited to investigating both general laws governing alternative designs for tree seedlings and the nature of trait adaptation in response to competition and environmental differences.

Keywords: Plant functional traits; Growth analysis; Optimal stomatal control; Optimization model; Trait evolution; Tree mechanics; Tree seedlings

1. Introduction

One of the most striking observations about plant communities everywhere is the high level of quantitative variation in functional traits among plant species both within sites (Westoby et al., 2002) and among sites (Niinemets, 2001; Wright et al., 2004; Maherali et al., 2004). This trait diversity is not only fascinating to naturalists, but also of ecological importance since it affects species distributions (Guthrie, 1989; Roderick et al., 2000; Prior et al., 2003) as well as ecosystem processes (Shugart, 1997; Díaz et al., 2004; Suding et al., 2005). Although progress has been made in understanding some dimensions of plant trait variation (Westoby et al., 2002; Reich et al., 2003), much still remains to be elucidated. Through an original application of an optimization modeling approach our study aims to improve this understanding.

* Corresponding author. Tel.: +1 514 398 4116; fax: +1 514 398 5069.
E-mail address: cmarks@po-box.mcgill.ca (C.O. Marks).

0304-3800/$ – see front matter © 2005 Elsevier B.V. All rights reserved.
doi:10.1016/j.ecolmodel.2005.09.011

We chose an approach based on optimization since optimization models have important advantages over more empirical and statistical models in investigating patterns of trait variation (Maynard Smith, 1982; Mooney and Chiariello, 1984; Givnish, 1986a; Parker and Maynard Smith, 1990; Farnsworth and Niklas, 1995; Mäkelä et al., 2002; Sutherland, 2005). Most significantly, optimization models are derived from first principles (Parker and Maynard Smith, 1990; Sutherland, 2005), which allows the mechanisms underlying plant function to be investigated directly. Furthermore, since first principles apply generally, optimization models can be used to make predictions about responses under new conditions (Sutherland, 2005).

These advantages have allowed optimization models for particular elements of plant function to provide insights into diverse aspects of plant function: nitrogen allocation (Hilbert et al., 1991; Van der Werf et al., 1993; Hikosaka and Hirose, 1998; Buckley et al., 2002), root-to-shoot ratio (Orians and Solbrig, 1977; Schulze et al., 1983; Hilbert, 1990; Chen and Reynolds, 1997; Stuefer et al., 1998; Magnani et al., 2002), shoot architecture (King, 1981, 1990; Niklas, 1994c), specific and canopy leaf area (Schieving and Poorter, 1999; Farquhar et al., 2002), stomatal control (Cowan and Farquhar, 1977; Hari et al., 1986; Givnish, 1986b; Mäkelä et al., 1996), and water-use (Schwinning and Ehleringer, 2001; Zavala, 2004). To advance this line of inquiry, we have developed a more holistic optimization model, the Tree seedling Adaptive Designs (TAD) model that considers a broad array of elements in plant function influencing tree seedling growth and survival. Here we present the TAD model as well as demonstrating its realism with a particular focus on seedling growth analysis.

TAD advances plant optimization models in four important ways. First, while fitness is known to be affected by multiple traits and may be limited by multiple resources (Mooney and Chiariello, 1984; Körner, 1991; Gutschick, 1999), TAD is to our knowledge the first optimization model to incorporate key traits associated with the economy of all four primary resources for plant growth: water, nitrogen, light and carbon.

Second, many plant organs perform multiple tasks and consequently their traits must reflect a compromise optimizing performance across a set of individual tasks (Mooney and Chiariello, 1984; Körner, 1991; Farnsworth and Niklas, 1995; Gutschick, 1999). Few optimization models have addressed the challenge of multiple plant functions, and those that have typically used a multi-objective optimization approach which is difficult to justify biologically (Niklas, 1994c). A more elegant solution is to integrate multiple functions into a single fitness measure as in TAD where growth rate is maximized, but with prevention of carbon starvation, dehydration, and mechanical failure acting as constraints. The combination of survival and maximization of growth is a well accepted fitness measure for tree seedlings, since maximal seedling growth increases the chance to survive into adulthood and increases lifetime reproductive potential (Van Valen, 1975; Harcombe, 1987; Oliver and Larson, 1996; Landis and Peart, 2005). Thus the fitness measure in TAD is biologically realistic and can be easily interpreted.

Third, the variation in individual traits cannot be fully understood without taking into account the direct and indirect effects of other traits (Mooney and Chiariello, 1984; Körner, 1991; Gutschick, 1999). In other words, the conclusions from studying traits at the organ level in isolation do not necessarily scale up to the whole plant. For example, the values for leaf traits that maximize nitrogen-use-efficiency at the leaf level are not the same as the values for leaf traits that maximize nitrogen-use-efficiency at the whole plant level (Aerts and Chapin, 2000). This interdependence requires taking a whole plant approach. Furthermore, ecophysiology can be directly linked to population and community ecology only at the whole-plant level of trait organization (Mooney and Chiariello, 1984). Some other optimization models recently have moved toward this holistic approach (Schwinning and Ehleringer, 2001; Zavala, 2004), but not as comprehensively as TAD.

Fourth, plant traits modify the environment and thereby also the selection on traits (Van Valen, 1977; Laland et al., 2004). In TAD these feedbacks on the environment are modeled in a spatially explicit manner. Consequently TAD is capable of accounting for the effects of neighbor–neighbor competition. Some previous optimization models (Cohen, 1970; Iwasa et al., 1984; King, 1990, 1993; Schieving and Poorter, 1999; Schwinning and Ehleringer, 2001) have also included these feedback effects, but none has considered competition for light, nitrogen, and water all at the same time. Because of this and also the preceding points, TAD represents a significant advance in optimization modeling

of the contribution of interacting traits to variation in plant function.

2. Model introduction

The holistic approach of the TAD model results in a truly complex system of trait interactions. Consequently the TAD model has a relatively large number of trait variables even though each individual tradeoff was modeled as simply as possible. Specifically, the TAD model is based on the interactions, and particularly the tradeoffs, among 34 functional traits critical to seedling growth (listed in Table A1 in Appendix A). These 34 traits were selected based on a thorough review of the literature on the functional ecology of woody plants. The primary criteria for making a trait subject to optimization in the TAD model was that (a) the trait has a substantial effect on a tradeoff affecting one of the four resources included in TAD and (b) this tradeoff was sufficiently well understood and quantified to model with reasonable accuracy. Since the values of the 34 traits are jointly optimized in the model, we refer to these 34 traits as *independent* traits in contrast to other *dependent* traits that can be derived from the values for these 34 traits. Functional traits that did not derive from the independent traits nor meet our criteria for inclusion as independent variables were set to a constant value in the current version of the TAD model. Since leaves have been studied much more intensively than roots, the current version of the model has a more detailed representation of aboveground than belowground traits, but many belowground traits and processes are included. The 34 independent traits include four parameters related to seed reserve allocation, six parameters related to carbon allocation, three parameters involved in nitrogen allocation, three parameters for stomatal control, nine leaf traits, five root traits, and four wood traits.

The simultaneous optimization of the 34 independent traits in the TAD model requires a powerful numerical technique. We chose a genetic algorithm (GA) for this purpose (Goldberg, 1989; Mitchell, 1996). In addition to their efficiency as an optimization technique, GAs are attractive because of their similarity to some key aspects of biological evolution (Farnsworth and Niklas, 1995; Wagner and Altenberg, 1996). In fact GAs were initially developed in analogy to biological evolution (Goldberg, 1989). Specifically, as in biological evolution, the efficiency of GAs derives from the interaction of selection and recombination of trait value combinations over many generations where each subsequent generation builds on the best trait combinations of the previous one until an optimum is reached (Goldberg, 1989). Consequently GAs can mimic in a general way the effect of history on evolutionary outcomes (Farnsworth and Niklas, 1995; Wagner and Altenberg, 1996).

The model outcomes found by the GA represent optimal design solutions constrained by the tradeoffs and interactions among the independent traits. In the case of TAD only phenotypic constraints could be modeled since the genetic controls of most functional plant traits are currently not sufficiently well described to include any genetic constraints (Geber and Griffen, 2003). The solutions found with the GA in the TAD model thus represent potential optimal tree seedling designs from a strictly phenotypic perspective.

Given that the functional tradeoffs and interactions among the 34 independent traits are the defining characteristics of the TAD model, in the following paragraphs we provide a brief summary of these tradeoffs in the context of the plant organs involved. This introduction focuses on outlining the tradeoffs and particularly on demonstrating how the different tradeoffs are interconnected through the multifunctional roles of individual traits. The equations showing precisely how the 34 independent traits fit into this complex network of interactions are described in the subsequent section, which also gives the detailed references justifying our models of individual tradeoffs.

2.1. Leaves

Leaves are the main center of activity for plants, and consequently many plant activities are interconnected there. For example, the gas exchange occurring in leaves connects the plant's carbon economy with its water economy. Specifically, leaves have stomatal pores in their epidermis to regulate gas exchange between the leaf and the surrounding air. A plant may increase stomatal conductance allowing more CO_2 to diffuse into the leaf, thereby increasing the photosynthetic rate, but only by simultaneously increasing the amount of water lost from the leaf through transpiration. Since supplying the leaf with

water is costly in terms of increased construction of roots for water absorption and stem wood for its conduction, a plant should regulate its stomatal conductance such that it maximizes photosynthesis relative to transpiration. Leaves also have a cuticle to reduce water losses. Investing in a thicker cuticle improves survival during a prolonged drought, but also increases leaf construction cost and thereby carbon expenditure.

This tradeoff between water loss and carbon uptake is also affected by the internal anatomy of the leaves. Increasing the number of mesophyll cell layers increases the photosynthetic capacity, while at the same time reducing transpirational water losses from the leaf since these are proportional to leaf surface area. In other words, increasing the number of mesophyll cell layers potentially increases the water-use-efficiency. However, upper layers of mesophyll cells shade lower layers, preventing them from getting sufficient light for photosynthesis, especially if the leaf is in low light conditions. Consequently, there is a link between tradeoffs related to light and tradeoffs related to leaf gas exchange.

The thickness of the leaf cell walls also affects this internal shading. However the cell walls must have a minimum thickness relative to the cell diameter to withstand the cell's turgor pressure without rupturing. The turgor pressure is proportional to the osmotic potential and this osmotic potential in turn critical to the plant's ability to draw in water at low soil moisture. Thus the availability of water constrains the minimum cell wall thickness. Furthermore, like cuticle thickness, the thickness of the cell walls affects the leaf construction cost thereby creating another link to the carbon economy.

Similarly, leaves may contain varying amounts of sclerenchyma. Sclerenchyma increases the strength of a leaf. Similarly the thickness of mesophyll cell walls relative to mesophyll cell diameter increases the strength of the leaf, although sclerenchyma is 10 times as strong on a cross-section basis. In general, the longevity of leaves is a function of their strength, presumably to resist mechanical damage by herbivores or wear and tear from wind. The disadvantages of investing in sclerenchyma are that this reduces photosynthetic capacity slightly by increasing internal shading in the leaf as well as increasing construction cost. Thus sclerenchyma and mesophyll wall thickness mediate a tradeoff between leaf durability and carbon investment in leaf construction.

Finally, the photosynthetic capacity of individual mesophyll cells in the leaves depends on the number of chloroplasts that they contain. More chloroplasts increase photosynthetic capacity, but also increase internal shading, maintenance respiration rate, and levels of nitrogen investment. Thus mesophyll cell design also links the water, light, and carbon economies with the nitrogen economy of the plant. Clearly these tradeoffs associated with leaf design alone already represent a complex system of interactions involving all four modeled resources.

2.2. Stems, branches, and thick roots

This system of interactions becomes even more complex when the tree's structural organs are considered. Leaves and the structural organs are functionally linked. Leaves provide the structural organs with the carbon necessary for growth and maintenance, while the support structures provide the leaves with the water, nitrate, and light that are needed for continued carbon assimilation. For example, the total stem cross-sectional area affects the stem's hydraulic conductance, but also increases its construction cost. The advantage of a higher stem conductance is a higher rate of water supply to the leaves and consequently higher photosynthetic rates. Alternatively, if leaves increase water-use without adequate stem conductance, then xylem water potentials could drop substantially. To withstand these lower water potentials the xylem conduits need to have thicker cell walls to guard against implosion in the case of cavitation, which increases carbon investment costs per conduit.

The thickness of the conduit walls relative to conduit diameter also determines the density of the wood and thereby also its strength. Thus there is a direct link between xylem hydraulics and stem mechanics, with important implications for light capture. In particular, the structural organs need to have sufficient mechanical strength to support themselves as well as the leaves and any external loads imposed on them. To support this mechanical load the main thick roots, stem and branches need to increase in cross-section area, thereby increasing construction and maintenance costs. This carbon cost increases dramatically as the tree grows in height. However, height growth is necessary to extend

new leaf growth into the best light environment. This effect is particularly strong when neighboring plants are competing for light. Thus as in leaf design, the design of structural organs involves multiple tradeoffs and interactions among the carbon, water, and light economies which further increases complexity in the network of interactions among traits.

2.3. Fine roots

Much as in leaves, in fine roots there are tradeoffs among resource uptake, nitrogen investment, and maintenance costs. Specifically, fine roots can have a greater investment in metabolic activity associated with higher nitrogen content and higher nutrient uptake rates, but this also increases their maintenance respiration. There is also a belowground analogy to the tradeoff between the costs of extension growth and access to light. In particular, fine roots can be distributed primarily in the upper soil layers where nitrate is most abundant but where evaporation is also greater or in deeper soil layers where they can avoid competition and moisture availability is typically greater. Thus belowground there is a three-way tradeoff among nitrate uptake, water uptake, and carbon costs for root construction.

2.4. Whole seedling

The pattern emerging from this sketch of tradeoffs in tree seedling design is that no tradeoff acts entirely in isolation of other tradeoffs—a complex network of interactions among traits arises because many traits have multiple functional connections associated with more than one tradeoff. Furthermore, the economies of the four main plant resources are interacting in multiple ways both within the functioning of an individual organ and through interactions among organs. Consequently the design constraints for tree seedlings represent a complex system, and complex systems are known to behave in fundamentally different ways from their individual components (Bossomaier and Green, 2000; Ellis, 2005). In the case of the TAD model that means that the type of trait variation expected in response to an environmental difference based on considering a single tradeoff in isolation at the organ level may not be the same as when considering an ensemble of tradeoffs at the whole plant level. The holistic approach taken in the development of the TAD model thus provides an opportunity to potentially gain new insights into the causes of trait variation in nature. This potential for emergent properties due to complex interactions is what sets the TAD model apart from more traditional models optimizing only an isolated element of plant function.

2.5. Limitations

As is the case for any model, the TAD model has both strengths and weaknesses that reflect our modeling goals and objectives. We place a premium on strengthening our understanding of the interactions among traits that influence growth and survival within a fairly normal range of environmental conditions associated with upland forests within a climate zone. Our focus is on the uptake and use of resources for growth, not on factors that define latitudinal range limits or that decide survival of episodes of severe environmental stress. Specifically, the TAD model is not addressing questions of cold hardiness, salt tolerance, or flood tolerance (soil anoxia). In any case, the tradeoffs associated with adaptations for surviving these severe environmental stress factors often are still too poorly understood for inclusion in the tradeoffs organizing the model. Thus, in its present form, the TAD model cannot be applied in extreme environments such as the arctic tree line or a mangrove swamp. Nor can the model address the distribution of species along an environmental gradient involving any of these critical stresses. The TAD model is appropriate, however, for making predictions about the nature of trait adaptation in tree seedlings growing in upland forests within a climate zone, which is sufficient to this early stage of our investigations.

At this stage in its development, the TAD model also does not address questions of phenotypic plasticity and its potential influence on the evolution of trait complexes (Pigliucci, 2004). Real tree species are usually growing over a range of environments and there is often some degree of gene flow between local populations within this range. This environmental heterogeneity would prevent the species from becoming perfectly adapted to any one of the local environments as well as selecting for plasticity in individual traits (Sultan and Bazzaz, 1993a, 1993b, 1993c). However, at this point, we are interested only in investigating the simpler case of adaptation to a single environment. Furthermore, the costs of plasticity are still not understood (Pigliucci, 2005). Thus as in other trait optimization models, the

possible effects of selection for performance in multiple environments are set aside.

Finally it is important to note that TAD in particular and optimization models more generally are ideally suited as *investigative* models, as opposed to *predictive* models (Parker and Maynard Smith, 1990; Sutherland, 2005). In predictive models the emphasis is on accurately modeling a particular species in detail, whereas in investigative models priority is given to generality. For example, when the purpose of the model is to accurately forecast the yield of a crop as in agronomic or silvicultural research, then a predictive model is most suitable (Perttunen et al., 1996; Genard et al., 1998). To achieve this accuracy, predictive models rely on greater empiricism that obscures the underlying mechanisms (Parker and Maynard Smith, 1990; Sutherland, 2005). Consequently, predictive models are unsuitable to investigating the general evolutionary causes of variation in tree designs. Empirical models can at most give some limited insights into the effect of trait variation in the immediate vicinity of the current value by doing a parameter sensitivity analysis. In contrast, investigative models sacrifice some empirical accuracy in favor of the greater generality that can be achieved by focusing on the underlying tradeoffs that govern trait variation. In other words, the predictions of investigative models are derived from first principles (Sutherland, 2005). This mechanistic basis of optimization models allows their predictions to be generalized across the full breadth of present day tree seedling designs as well as extinct and potential future designs.

3. Model description

The following subsections give the detailed, fully referenced description of the seedling simulation model including all equations and assumptions. Symbols used in equations are defined where they are first used, and also are summarized in Appendix A.

3.1. Spatial representation

The model makes two simplifications that reduce computational effort substantially. The first is that space is divided into grid cells (Fig. 1). Each grid cell can contain a cluster of leaves and twigs or a block of soil and roots. This aggregated representation is simpler than in models where leaves and roots are represented individually (for example, LIGNUM, Perttunen et al., 1996). The advantage of this aggregate approach is that simulations require much less memory and run more quickly; the disadvantage is that some questions related to seedling architecture cannot be investigated.

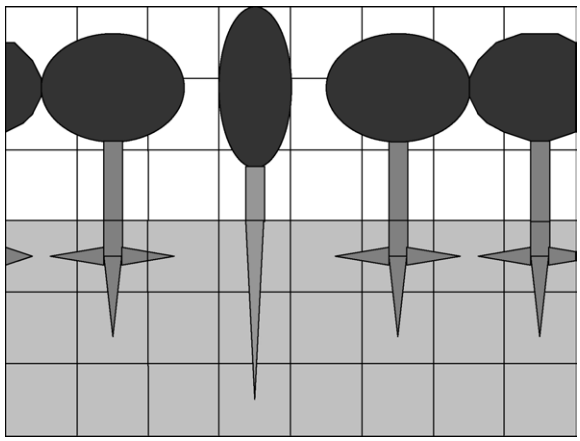

Fig. 1. Grid cell representation of seedlings and environment in the TAD model. The face of each grid cell is 30 cm × 30 cm and each cell has a nominal depth of 30 cm. The particular example illustrated schematically here shows a case where two different seedling designs are competing with each other; note that in the actual simulation there is a repeating boundary condition horizontally to avoid edge effects.

A second simplification is that a vertical slice through the seedling population represents the environment where neighbor–neighbor interactions occur. As shown Fig. 1, the space in the model consists of a wall of grid cells that are stacked on top of each other like blocks. In this representation, the units are the same as in nature in that the wall of grid cells has a nominal depth (30 cm), but interactions basically are reduced to two dimensions: the vertical direction and only one horizontal direction. Since it is reasonable to assume that the interactions in the second horizontal direction would be similar to the first, this simplified representation can reproduce natural seedling-seedling and seedling-environment interactions. The great advantage of using a 2D instead of a 3D array of grid cells, of course, is that computational effort is greatly reduced not just because fewer grid cells are needed but also because fewer seedlings need to be simulated to assess competitive interactions. Another advantage of using a grid cell representation is that resource levels can be calculated as a balance of flows into and out of grid

cells. Thus only neighboring cells need to be considered when calculating available resource levels. For example, in many conventional models, light intensity calculations check for obstructions to light in every direction and then sum the light rays coming from the unobstructed directions, whereas here irradiance is simply the sum of radiation coming from the immediately neighboring cells directly and diagonally above. Without these simplifications the novel multiple-trait approach in the TAD model would not have been feasible using current computers (1–2 GHz); the reduced dimensionality and aggregation do not compromise the basic questions we wish to investigate.

3.2. Seedling spacing and initial size

Normally in TAD, there is a row of four seedlings in each growth simulation to include the effects of neighbor–neighbor competition as illustrated in Fig. 1. However, TAD also gives the option to run the growth simulations without competing neighbors, in which case the grid would contain only one seedling. In the default case of competing neighbors, the seedlings are spaced at every second grid cell (i.e. 60 cm apart). To avoid edge effects and ensure symmetry in the horizontal direction there is a repeating boundary condition. In other words, one could consider the right side of the grid as connected to the left side of the grid as if the grid were on the surface of a cylinder, or alternatively one could consider that there are an infinite number of identical copies of the grid repeating in the horizontal direction. At the beginning of the simulation each seedling only occupies one above ground and one below ground grid cell. The initial seed size is specified in the program and kept constant for all simulations, but these initial seed resources can be allocated differently in the germinant. There are four independent traits specifying this initial allocation. The first specifies the proportion allocated to below ground versus above ground parts (root-to-shoot). The second specifies the proportion allocated to fine roots versus thick roots (fine-to-thick). The third specifies the proportion allocated to leaves versus stems and branches (leaf-to-stem). The fourth is the fraction allocated to storage that the seedling can use to cover maintenance costs in subsequent days. A dry mass of 1.0 g was chosen for the initial seed size (Young and Young, 1992) with a composition of 50% carbon, and 8% nitrogen (our unpublished data).

3.3. Environment

Details of how environment is described in the TAD model are given in the following numbered subsections: (1) weather, (2) nutrient input, (3) evaporation, (4) light interception and distribution, (5) atmospheric CO_2 concentration, and (6) soil resources.

3.3.1. Weather

The weather in the simulations varies on two time scales. There is (1) a variation from 1 day to the next that follows a prescribed time series and (2) a fixed diurnal variation. The prescribed time series is generated from a statistical distribution that imitates natural randomness, and the same time series is used in each simulation for a given environmental regime to avoid statistical noise in the results. The diurnal variation follows the same basic pattern every day and is simply scaled in magnitude by the level for that day in the day-to-day time series. For example, the value from the light intensity time series gives the average light intensity for the particular day and this average intensity is used to scale the diurnal curve of light variation. Different time series can be used as specified by the user. For example, if the user is interested in a light treatment then there is a choice of light time series each with a different range of light intensities. The distributions and ranges for the different weather time series are summarized in Table 1. There are five time steps for diurnal variation in weather: early morning (3 h), late morning (3 h), early afternoon (3 h), late afternoon (3 h), and night (12 h). The distribution of light also changes direction over the course of the day, as it does in nature.

3.3.2. Nitrate input

The nitrate input is a constant user-specified rate (g nitrogen/m^2/day). This nitrate input is added to the topsoil layer daily over the simulated period of growth. In nature, nutrient inputs are influenced by many variables such as temperature, soil moisture, and litter type. In this model, nitrate input was intentionally kept separate from these other variables so that truly independent nitrate treatments could be applied in the simulations.

3.3.3. Evaporation

Evaporation occurs only from the top layer of soil grid cells. The rate of evaporation is constant

Table 1
Ranges for weather data for different treatments in simulated experiments

Variable	Distribution	Range
Temperature (°C)	Normal	Low: mean 22, max 28.2, min 16.6 High: mean 27, max 33.7, min 20.1
PAR (μmol/m^2)	Uniform random	Ranges for the five light treatment levels: 1–20, 20–50, 50–200, 200–500, 500–1000
Relative humidity (%)	Uniform random	Ranges for the two humidity treatment levels: 50–75, 70–90

throughout the simulation since the effect of weather and soil moisture on evaporation pose complications that are not important to the main purpose of the model. Thus for simplicity a constant evaporation rate per soil area is specified and is a function of only the amount of water available in the soil

$$E_{\text{vap}} = \frac{E_{\text{daily}} S_{\text{grid}}}{\text{e}^{-2\Psi_{\text{soil}}}} \quad (1)$$

Evaporation (E_{vap}) declines exponentially with soil moisture to prevent the evaporative water loss from grid cells from exceeding the water available. The user specifies the constant E_{daily}. S_{grid} is the soil surface area and Ψ_{soil} is the soil water potential.

3.3.4. Light interception and distribution

The light incident at the top of the grid is assumed to be from three directions: directly from above and at 45° angles from left and right. The relative amount from each direction depends on the time of day, and the absolute amount on the weather input time series as explained above. The light incident to lower grid cells is the sum of the light incident to the three neighboring grid cells above (vertically and diagonally) minus the amount of light that is intercepted by foliage in those cells.

Light interception is modeled using an equation derived by Monsi and Saeki (1953):

$$I = I_0 \left(1 - \frac{s_{\text{leaf}}}{S_{\text{grid}}}\right)^n \quad (2)$$

where s_{leaf} is the effective area of a leaf, which depends on the direction of the light and the angle of the leaf. To simplify computations, all leaves were assumed horizontal, and uniformly and randomly distributed throughout the grid cell. The variable, I is the light intensity in the canopy, I_0 is the light intensity above the canopy grid cell, and n is the number of leaves in the grid cell.

The photosynthetic rate is calculated by assuming that the median light intensity within a grid cell is representative for the light intensity received by the leaves at the aggregated level of the grid cell. This approximation is calculated by setting n to half the total number of leaves in the grid cell. The light leaving the grid cell to enter the grid cell below is calculated by setting n to the total number of leaves in the grid cell. The number of leaves in the grid cell is calculated by dividing the total leaf area by the area of a leaf. The leaf size was constant in all simulations since the advantages of large leaf size are insufficiently well understood currently to make leaf size an independent variable in the model. An area of 64 cm^2 was chosen as representative of an average size leaf based on our unpublished data for seedlings of 26 temperate deciduous hardwood tree species.

3.3.5. Atmospheric CO_2

The atmospheric concentration of carbon dioxide is an important resource and is known to have played an important role in the evolution of plants (Bateman et al., 1998; Willis and McElwain, 2002). In the model, the user can set the atmospheric CO_2 concentration. It remains constant throughout the simulation and affects the rate of photosynthesis as will be explained in the section on leaf gas exchange.

3.3.6. Soil moisture

As with the light calculations, the calculations for the water available in the soil make use of the grid cell approach. The water contained in a grid cell is simply the balance between the uptakes by the seedlings roots and the water added to the cell. Water is added to all of the soil grid cells at the beginning of the simulation and is subsequently replenished at a user-specified interval. At each water addition, the soil moisture reaches

some user-specified percentage of saturation. Rather than requiring rewetting of the entire soil profile each time, the model has an option to impose a vertical profile where only the topmost layer of soil grid cells is rewetted each time, the second layer every second time, the third layer every third time, etc. The program also permits setting a drought period where rewetting is suspended for a user-specified number of days, starting at a user-specified day within the simulated growth period. After the water balance has been computed for a grid cell, the volume fraction of water remaining may be used to compute the water potential of the soil (Ψ_{soil}), and its specific conductance (ε), using empirical curves relating specific conductance and water potential to the volume fraction of water in the soil. The curves for typical clay, sand, and loam soils were taken from Brady and Weil (1999) and programmed into TAD using piecewise, linear approximations. The user specifies if the soil is to be a sand, loam or clay during the growth simulations. This choice of soil type also determines the water holding capacity of the soil, as it does in natural soils.

3.4. Tree seedling traits and trait tradeoffs

The following subsections discussing the trait tradeoffs are organized by function: (1) photosynthesis, (2) water conduction and mechanical support, and (3) soil resource uptake. Associated with each of these functions is a type of plant organ: (1) leaves, (2) stem, branches and thick roots, and (3) fine roots, respectively. In all cases the structures performing these functions have a construction cost, which will be discussed in Section 3.5.

3.4.1. Leaves (photosynthesis and transpiration)

Much of the internal anatomy is included in modeling the leaves. In particular, the mesophyll is approximated by several layers of spherical cells (as shown in Fig. 2) following the approach of Nobel (1991). Of course, strictly speaking, the mesophyll cells are not spherical, particularly the palisade cells, but this simplification does not change the fundamental nature of the tradeoffs and is thus a convenient way to simplify the model. Mesophyll cell diameter and cell wall thickness are independent traits in the model as well as the nitrogen concentration of the mesophyll cell contents. Epidermal cells are assumed to have the same diameter as mesophyll cells, but are assumed not to contribute to photosynthesis. The thickness of the cuticle may vary and affects minimum transpiration. Stomata are not modeled explicitly, but are included implicitly via stomatal conductance.

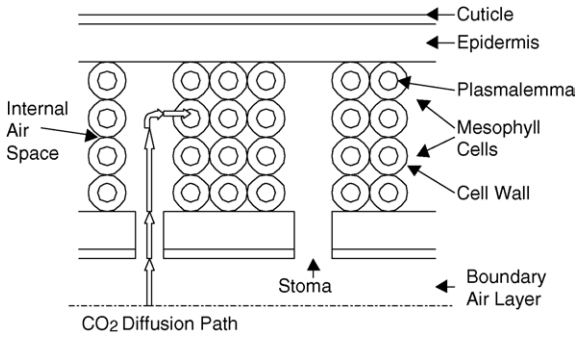

Fig. 2. Schematic diagram of a cross-section of a model leaf (thicker, open arrows indicate the diffusive pathway for CO_2).

3.4.1.1. Leaf gas exchange and optimal stomatal control. Fig. 2 illustrates the simplified representation of a leaf in the TAD model. The mesophyll cells are represented by spheres, and the diffusion pathways for CO_2 entering the leaf are indicated by arrows. Each of these pathways has resistances to diffusion associated with it. Differences in these resistances and especially in the number of layers of mesophyll cells are of great functional importance (Nobel, 1977, 1980).

To simplify the algebra in the derivations that will follow, the boundary layer conductance (g_b) and stomatal conductance (g_s) were combined into a single conductance (g_c):

$$g_c = \frac{g_s g_b}{g_s + g_b} \quad \text{or} \quad g_s = \frac{g_c g_b}{g_b - g_c} \tag{3}$$

Building on the approach of Hari et al. (1986), the model assumes that all the CO_2 fluxes are in equilibrium. Thus

$$g_i(c_i - c_{c,n}) = P_n \tag{4}$$

$$g_c(c_a - c_i) = \sum_n P_n = A \tag{5}$$

where g_i is the internal CO_2 conductance, c_i is the CO_2 concentration in the leaf internal air space, and $c_{c,n}$ is

the CO_2 concentration inside the mesophyll cells in the nth layer of mesophyll cells. P_n is the photosynthetic rate of the nth mesophyll layer, and A is the total photosynthetic rate for all of the mesophyll layers. All of the variables in Eqs. (4) and (5) are expressed per unit leaf area.

The model assumes that the photosynthetic rate of a mesophyll cell can be approximated by a function of the CO_2 concentration, $c_{c,n}$, and the light intensity inside the cell, $f(I_n)$.

$$P_n = c_{c,n} f(I_n) \tag{6}$$

The dependence on light intensity is modeled with a Michaelis–Menten function.

$$f(I_n) = \frac{I_n \nu_{\text{light}}}{k_{\text{light}} + I_n} \tag{7}$$

where I_n is the light intensity inside the leaf at the nth mesophyll layer, ν_{light} is a measure of the maximum photosynthetic capacity of the individual mesophyll layer that depends on the nitrogen content of the mesophyll cells (see Eq. (21)), and k_{light} is the constant expressing the response to light.

These functions that model CO_2 uptake at the individual mesophyll cell level are analogous to the functions that Hari and Mäkelä used to model CO_2 uptake at the whole-leaf level (Hari et al., 1986; Mäkelä et al., 1996). The whole-leaf view was avoided in the model because newer studies have shown that variation in internal leaf structure varies consistently with environmental gradients (Roderick et al., 2000; Niinemets, 2001; Wright and Westoby, 2002) and with leaf photosynthetic capacity (Nobel, 1977, 1980, 1991; Patton and Jones, 1989; Roderick et al., 1999a, 1999b).

Substituting Eq. (6) in Eq. (4) above, and solving for $c_{c,n}$, and then substituting back into Eq. (6) gives the following equation for the photosynthetic rate of mesophyll layer n, P_n:

$$P_n = \frac{g_i c_i f(I_n)}{g_i + f(I_n)} \tag{8}$$

This expression for mesophyll cell photosynthesis may be substituted in Eq. (5) and solved for c_i. This expression for c_i can then be substituted back into Eq. (5) and simplified to obtain the following equation for leaf photosynthesis per area, A:

$$A = \frac{g_c c_a \sum_n [g_i f(I_n)/(g_i + f(I_n))]}{g_c + \sum_n [g_i f(I_n)/(g_i + f(I_n))]} \tag{9}$$

or

$$A = \frac{c_a \sum_n [g_i f(I_n)/(g_i + f(I_n))]}{1 + (g_s^{-1} + g_b^{-1}) \sum_n [g_i f(I_n)/(g_i + f(I_n))]} \tag{10}$$

or

$$A = \frac{g_c c_a S}{g_c + S} \tag{11}$$

where

$$S = \sum_n \frac{g_i f(I_n)}{g_i + f(I_n)} \tag{12}$$

The transpiration rate, E, is assumed to be a function of only the stomatal (g_s), cuticular ($g_{\min}$), and boundary layer (g_b) conductances. Assuming that the stomatal conductance is in parallel to the cuticular conductance, and that both are in series with the boundary layer conductance yields the following equation:

$$E = \left(1.6 \left(\frac{g_b g_s}{g_b + g_s}\right) + \left(\frac{1.6 g_b g_{\min}}{1.6 g_b + g_{\min}}\right)\right) \Delta w \tag{13}$$

where the factor 1.6 accounts for the higher diffusion rate of H_2O in air than CO_2 in air. The Δw is the molar fraction gradient of water vapor from the substomatal cavity to the air, which is a function of humidity and temperature. Humidity is assumed to be saturated inside the leaf, and the humidity for the atmosphere is given by the weather inputs. The water vapor gradient also depends on the temperature of the leaf and the air temperature, which is influenced by the weather inputs as well. The leaf temperature is assumed to be 1, 3, 5, and 2 °C above air temperature for the four diurnal time steps in sequential order, and 1 °C below air temperature during the night.

The model uses the expression derived by Cowan and Farquhar for modeling stomatal control (Cowan

and Farquhar, 1977; Cowan, 1982). In this expression, the optimal variation of stomatal conductance is such that the partial derivative of transpiration with respect to photosynthesis is constant. This constant has been called the marginal cost of water, and is usually designated as λ. In TAD ν_{water}, the inverse of λ, is used in the computations

$$\frac{\partial E}{\partial A} = \lambda = \frac{1}{\nu_{\text{water}}} \quad \text{or} \quad \frac{\partial E/\partial g_s}{\partial A/\partial g_s} = \lambda = \frac{1}{\nu_{\text{water}}} \tag{14}$$

Since g_b is constant in the model, we can replace g_s with g_c to simplify calculation of the preceding partial derivatives from Eqs. (11) and (13)

$$\frac{\partial E}{\partial g_c} = 1.6\Delta w \tag{15}$$

$$\frac{\partial A}{\partial g_c} = \frac{c_a S^2}{(g_c + S)^2} \tag{16}$$

The preceding three equations can be combined to solve for the optimal conductance, $g_{c,opt}$

$$g_{c,opt} = S\left(\sqrt{\frac{c_a}{\Delta w 1.6\nu}} - 1\right) \tag{17}$$

or

$$g_{s,opt} = \frac{g_b(\sqrt{c_a/\Delta w 1.6\nu} - 1)S}{g_b - (\sqrt{c_a/\Delta w 1.6\nu} - 1)S} \tag{18}$$

The equation for $g_{c,opt}$ is analogous to the equation that Mäkelä et al. (1996) derived for the optimal stomatal conductance, but differs from it in two ways. Firstly, it includes the internal leaf conductance explicitly and takes into account the boundary layer and cuticular conductances. Secondly, the TAD model takes a different approach to calculating the marginal cost of water, λ, or its inverse, ν_{water}; this is discussed below.

Cowan and Farquhar (1977) did not derive a theory for the magnitude of λ and only show that it should be constant for short periods of time on the order of an hour or a day. Several solutions for calculating λ or more recently its inverse ν_{water} have been published since then (Cowan, 1982; Givnish, 1986b; Mäkelä et al., 1996). Of these the solution by Mäkelä et al. (1996) is the simplest for practical application. They calculate ν_{water} for a soil drying cycle as $\nu_{\text{water}} = p_0 e^{kt}$, where t is the time since the last rain, k is a species-specific constant, and p_0 is determined numerically such that all the available water in the soil is used up over an infinitely long drought period. This formulation represents an important theoretical advance, but is still not ideal for application in the inquiry that motivates the present model. Their approach assumes that when a rain occurs, the entire soil profile is wetted and that the cost of uptake is the same throughout the entire soil profile, but in the TAD model the spatial variation in soil moisture and root distribution is of critical interest. Furthermore, the TAD model can include competitive uptake of water by several plants with overlapping root systems and thus the optimal rate of water uptake depends on the uptake of competing plants as well as the time since the last rain. The strategy of competing plants likely differs between species, size classes and with any other asymmetries between the competitors. The degree of overlap of root systems and the soil properties affecting zones of influence of individual roots will moderate the degree to which competition affects ν_{water}. It is unreasonable to imagine that plants can gather all of this pertinent information on competitors and future weather directly, given that even human researchers with the aid of modern scientific instruments find this a challenging task. It is much more reasonable to assume that plants are reacting to competitors indirectly based on the soil moisture available in the rooted zone. Although the water status of the seedling's root zone is not a direct measure of statistical expectations of future competitor water use, evaporation and precipitation, it is likely correlated with them in a given environment. Plants can sense the local soil moisture status directly at individual roots (Khalil and Grace, 1993; Tenhunen et al., 1994; Loewenstein and Pallardy, 1998; Crocker et al., 1998) and soil moisture over the whole root zone indirectly via their own xylem water potential (Donovan et al., 2001). Although slight amounts of nocturnal transpiration may cause the predawn xylem water potential to be lower than the soil water potential, the parameters should still be correlated (Donovan et al., 2001). Therefore, we assume that in tree seedlings, ν_{water} is a function of the predawn xylem water potential at the base of the stem

$$\nu_{\text{water}} = c_1 e^{-c_2 \psi_x} \tag{19}$$

Avoidance of xylem cavitation has been shown experimentally to directly limit stomatal conductance

in several woody plant species (Cochard et al., 2002; Brodribb et al., 2003). Since cavitation is a threshold function of xylem water potential (Sperry, 1995, 2003), these experimental results reinforce the view of xylem water status as the key control variable for the regulation of transpiration. In a simulation model of plant water use Schwinning and Ehleringer (2001) also assumed a similar relationship where stomatal conductance depends exponentially on plant water potential. Furthermore, in the TAD model, the stomatal conductance is also limited by a maximum stomatal conductance, g_{max} that sets an upper limit to the stomatal conductance that is in turn another independent trait.

The cuticular conductance (g_{min}), also called minimum conductance because stomata do not close perfectly, varies by almost two orders of magnitude in nature and depends on cuticular thickness and permeability (Nobel, 1991; Kerstiens, 1996; Bargel et al., 2004). The thickness of cuticles varies from less than 1 μm to approximately 15 μm (Choong et al., 1992; Kozlowski and Pallardy, 1997), and the cuticular conductance varies approximately from 0.0005 to 0.0150 mol $H_2O/(m^2\,s)$ (see Table 8.1 in Nobel, 1991). Since cuticular transpiration is a diffusion process, a linear inverse relationship with thickness is expected of the following form (Bargel et al., 2004):

$$g_{min} = \frac{0.0075}{t_{cuticle}} \tag{20}$$

The constant 0.0075 was estimated by fitting Eq. (20) to the ranges of cuticular conductance and cuticle thickness in nature given above. The permeability of cuticles and the effect of residual transpiration through imperfectly closed stomata were assumed to be constant or negligibly different across species.

The parameter ν_{light} is a function of the leaf investment in nitrogen compounds, particularly in photosynthetic enzymes and chlorophyll

$$\nu_{light} = \frac{(N_{cell} - N_{min})}{m_{photo}} \frac{V_{mes}}{A_{mes}} \tag{21}$$

$$\frac{V_{mes}}{A_{mes}} = \frac{(\pi/6)d_{cell}^3}{d_{cell}^2} = \frac{\pi}{6} d_{cell} \tag{22}$$

where V_{mes} is the mesophyll cell volume and A_{mes} is leaf area taken up by a mesophyll cell. The parameter d_{cell} is the diameter of a mesophyll cell, which is an independent variable in the TAD model. The above relationship between maximum photosynthetic capacity and leaf nitrogen content is supported empirically within genera (Mooney and Gulmon, 1979; Niinemets et al., 2002) and across genera (Reich et al., 1997, 1998a, 1999; Shipley and Lechowicz, 2000; Wright et al., 2001, 2004; Westoby et al., 2002). The parameter m_{photo} estimates the slope of the relationship between nitrogen content and photosynthetic capacity at the level of an individual mesophyll cell layer. The minimum cell nitrogen concentration, N_{min} is subtracted from the cell nitrogen concentration, N_{cell} to account for the nitrogen invested in functions unrelated to photosynthesis.

The light intensity in mesophyll layer n, I_n, is different in each layer of mesophyll cells because of shading from layers above, and can be modeled as follows:

$$I_n = I_{in}(0.9)^{sc_w}(0.9)^{sc_{chl}} \tag{23}$$

where I_{in} is the incident light intensity on the leaf, and the internal shading coefficient due to cell walls (sc_w) and due to the chloroplasts (sc_{chl}) for layer z of mesophyll cells are calculated as follows:

$$sc_w = \frac{(2z+1)(c_w) + (z+1)(d_{cell} f_{scl}) + t_{cuticle}}{c_{shade1}} \tag{24}$$

$$sc_{chl} = (z-1)(N_{cell} - N_{min}) \left(\frac{\pi}{6} d_{cell}\right) c_{shade2} \tag{25}$$

where f_{scl} and $t_{cuticle}$ are independent variables representing the fraction of leaf cross-section area that is sclerenchyma, and the thickness of the leaf cuticle, respectively. The above shading coefficients (c_{shade1} and c_{shade2}) were estimated from measured internal light profiles (Cui et al., 1991) using the following assumptions. The reduction in light intensity was approximated as 20% after each layer of mesophyll cells in a typical leaf and that about half of that shading is due to cell walls and the other half due to the chloroplasts. Sclerenchyma tissue is assumed to have a shading effect similar to cell walls. Although this is an oversimplification of internal light profiles, this simplification approximates real light profiles reasonably well (Cui et al., 1991) and captures the essential nature of the tradeoffs.

The diffusion constant for CO_2 is given by Nobel (1991) as

$$D_{CO_2} = D^0_{CO_2}\left(\frac{T}{273}\right)^{1.8}\frac{P^0}{P} \quad (26)$$

where the pressure inside the leaf, P is assumed to be equal to the air pressure, P^0. T is the absolute temperature of the leaf. The constant $D^0_{CO_2}$ is equal to $1.4968 \times 10^{-9}\,m^2/s$ if diffusion is in water and $1.33 \times 10^{-5}\,m^2/s$ if it is in air. Following Nobel (Chapter 8 in Nobel, 1991), we can approximate the internal leaf resistances to CO_2 diffusion with these diffusion constants:

$$R_{ias} = \frac{z d_{cell}}{D^{air}_{CO_2}} \quad (27)$$

The resistance of the internal air space (R_{ias}) is based on the number of mesophyll cell layers, z, separating the mesophyll cell layer from the stomata (assumed to be on the bottom leaf surface only), and d_{cell} is the mesophyll cell diameter

$$R_{cw} = \frac{3(c_w)}{\pi D^{water}_{CO_2}} \quad (28)$$

The cell wall resistance (R_{cw}) is based on the cell wall thickness, c_w, and the diffusion constant is divided by three to account for the tortuosity of the path through the cell wall, a realistic approximation according to Nobel (1991)

$$R_{pl} = \frac{1000}{\pi} \quad (29)$$

The resistance of the plasmalemma is assumed to be constant as suggested by Nobel (1991)

$$R_{cy} = \frac{0.4 \times 10^{-6}}{\pi D^{water}_{CO_2}} \quad (30)$$

For the cytosol resistance (R_{cy}), a distance of 0.2 μm from the plasmalemma to the chloroplasts is assumed and the diffusion constant is estimated to be about half that in water (Nobel, 1991). The resistance of the chloroplasts is neglected in the model since it is assumed to be the same in all species.

These four resistances may be combined to give the internal leaf conductance, g_i

$$g_i = \frac{1}{R_{ias} + R_{cw} + R_{pl} + R_{cy}} \quad (31)$$

To increase photosynthesis, selection should favor reducing the resistances to CO_2 diffusion across the mesophyll cell walls by reducing the cell wall thickness, c_w, which is an independent trait in the model. However, there is a tradeoff with the strength of the cell walls needed to counterbalance the turgor pressure inside the cells that results from the cell osmotic potential.

3.4.1.2. Leaf osmotic potential. The osmotic potential of mesophyll cells is constrained by the ability of the cell walls to resist the internal pressure at full turgor. Approximating the cell as a spherical thin walled pressure vessel, the maximum osmotic potential is given by the following equation (Beer and Johnston, 1985):

$$\text{osm} = \frac{-8\,c_w \tau}{d_{cell}} \quad (32)$$

where τ is the shear strength of the cell walls.

In the TAD model, the leaf osmotic potential is used as an approximation for the minimum water potential that the leaf can sustain without wilting (wilting point). In real leaves, the water potential at the wilting point is slightly less than the osmotic potential at saturation, but the two are correlated if the effects of cell wall elasticity are neglected (Kramer and Boyer, 1995; Kozlowski and Pallardy, 1997). The water potential at wilting could be lowered by increasing the elasticity of the cell walls, but this effect is relatively small (Kramer and Boyer, 1995; Kozlowski and Pallardy, 1997). However, there is an advantage to decreasing the elasticity. For a given amount of leaf dehydration, a leaf with lower elasticity will result in a lower leaf water potential and thus larger pull on water from the soil than in a leaf with greater elasticity. Furthermore, the thick cell walls necessary to resist the high turgor pressures associated with low osmotic potentials inherently have a low elasticity (Niinemets, 2001). There is some debate around whether lower elasticity or lower osmotic potential at full turgor is more important to improving water uptake from drying soil (Niinemets, 2001), but in either case leaf cells need thick stiff walls. Therefore, the effects of elasticity were neglected in the present version of the

TAD model to keep it as simple as possible. As a consequence of the need for thick cell walls, species with lower osmotic potentials should also have higher leaf tissue density. The predicted relationship between leaf osmotic potential and tissue density has been observed experimentally (Sack et al., 2003). Thus there is a fundamental tradeoff between leaf construction cost (tissue density) and the ability to withstand low water potentials.

3.4.1.3. Leaf longevity. Leaf life span is closely correlated with leaf mass per area (LMA) (Eamus and Prichard, 1998; Wright et al., 2002; Wright and Westoby, 2002). Most researchers believe that a large investment in thick cell walls and sclerenchyma (i.e. high LMA) increases the strength of the leaf, hence increasing its resistance to tearing by wind or herbivores and increasing leaf durability (Choong et al., 1992; Lucas et al., 2000). Using the data for dry sites from Wright and Westoby (2002) as a guide (data with a range in leaf longevity of 10–200 weeks), the following relationship was estimated:

$$L_{\text{long}} = \frac{(\pi d_{\text{cell}} c_{\text{w}}(n+2) + 10 f_{\text{scl}}(n) d_{\text{cell}}^2)}{100} \quad (33)$$

This relationship assumes that sclerenchyma is about 10 times as strong on a cross-sectional area basis as cell wall tissue (Choong et al., 1992). We assume the relationship is linear, which is reasonable given that the slope of the regression line was 1.2 in the data (Wright and Westoby, 2002).

3.4.2. Stems, branches, and thick roots (water transport and mechanical support)

The model considers both the function of wood in supporting the tree mechanically and in conducting water to the leaves.

3.4.2.1. Xylem hydraulic conductance. The root and branch conductance, respectively, are calculated as:

$$K_{\text{r}} = \frac{\beta_{\text{r}} \kappa_{\text{xy}}}{L_{\text{r}}} \quad (34)$$

$$K_{\text{b}} = \frac{\beta_{\text{b}} \kappa_{\text{xy}}}{L_{\text{b}}} \quad (35)$$

where β is the cross-sectional area, L is the path length, and κ_{xy} is the xylem conductivity (i.e. conductance per area). Conductivity depends mostly on the diameter of xylem conduits, and to a lesser degree on the constrictions between conduits called pits (Hacke and Sperry, 2001; Sperry, 2003). However, the tradeoffs involved are still not fully understood and quantified (Hacke and Sperry, 2001; Sperry, 2003). Therefore, the xylem conductivity is taken as a constant in the TAD model. The user can set the xylem either as conifer xylem (entirely made of tracheids), or angiosperm xylem (made of vessels, tracheids, and fibers). The conductivity (κ_{xy}) was set to 2 and 4 kg/(s m MPa) for tracheid and vessel xylem, respectively, values that are typical for the middle of the respective ranges of values in natural trees (Sperry, 2003). In the simulations for the first project presented here the xylem type was set as the angiosperm type.

3.4.2.2. Minimum xylem water potential. Since a continuous supply of water to the leaves is essential for their survival, it is crucial that when a conduit cavitates the embolism does not spread to neighboring conduits. The geometry of the pits controls the lowest water potential that the xylem can sustain without cavitation. The design of the pits has evolved to match the minimum water potential experienced by a woody plant in its normal habitat (Sperry, 2003). However, when a conduit does become embolized, not only must the pit be able to prevent the bubble from spreading, but the xylem wall must also be able to sustain the pressure difference across it, as illustrated in Fig. 3. Since the strength of the walls is mostly a function of their thickness, the density of wood should be related to the water potential at cavitation (Hacke et al., 2001). Empirical

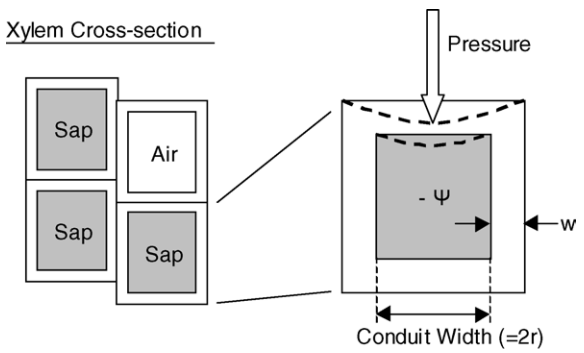

Fig. 3. Cross-section of xylem conduits illustrating wall deformation in response to cavitation of a neighboring conduit.

relationships between water potential at cavitation (Ψ_x) and wood density (ρ_x) or the ratio of wall thickness to conduit width have indeed been found in temperate trees (Hacke et al., 2001). This trend of decreasing minimum water potential (measured in leaves) with increasing wood density was also evident in tropical trees (Borchert, 1994; Meinzer, 2003). The empirical relationships found by Hacke and Sperry (2001) and, that are used in the TAD model differ between gymnosperms and angiosperms.

For gymnosperms (tracheids only):

$$\Psi_{x,\min} = -50\left(\frac{w}{r}\right)^2 \tag{36}$$

$$\rho_x = \left[1 - \left(\left(\frac{w}{r}\right)0.5 + 1\right)^{-2}\right]\frac{0.94}{0.48}, \quad \text{where} \quad \frac{w}{r} \leq 0.50 \tag{37}$$

For typical angiosperms (mostly vessels and fibers):

$$\Psi_{x,\min} = -167\left(\frac{w}{r}\right)^2 \tag{38}$$

$$\rho_x = \left[1 - \left(\left(\frac{w}{r}\right)0.79 + 1\right)^{-2}\right]\frac{1}{0.32}, \quad \text{where} \quad \frac{w}{r} \leq 0.23 \tag{39}$$

3.4.2.3. Branch architecture. The simple 2D grid cell approach of the model that treats leaves and fine roots as clusters rather than as individuals is not conducive to studying architectural detail, and architecture is therefore held constant in the TAD model. Fig. 4 illustrates the simplified representation of canopy architecture, which consists of vertical stem segments and horizontal branch segments.

In addition to this mechanical architecture, plants have a hydraulic architecture. The ratio of stem cross-sectional area to leaf area is called the Huber value (HV) and it is commonly employed in experimental studies of tree hydraulic architecture (Tyree and Ewers, 1991). In the TAD model the independent trait x_{sect1} is similar but not the same as the Huber value. The value of x_{sect1} is defined as the minimum amount of branch cross-section area per leaf area, when new leaves are grown. Since leaves can die subsequently, the actual Huber value can be larger than x_{sect1}. Furthermore, as shown in Fig. 4, x_{sect1} increases towards the base of the stem due to stem taper, which is also seen in natural trees (Mencuccini, 2002). The amount of this stem taper is also an independent trait in the TAD model. Analogous to x_{sect1} there is another independent variable x_{sect2} defined as the minimum amount of thick root cross-section area per fine root length.

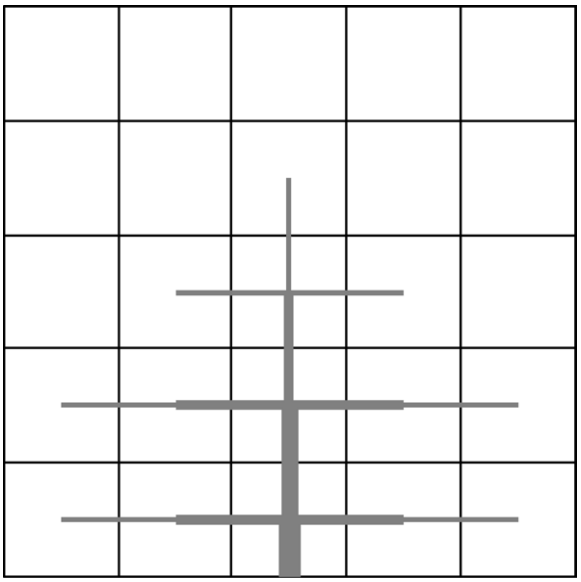

Fig. 4. simplified representation of seedling architecture inside the model grid.

Beyond this coarse-scale crown architecture, trees need fine-scale architecture to display the individual leaf blades within a grid cell. In natural woody plants, this fine-scale architecture consists of a combination of twigs and petioles (or rachises in the case of compound leaves). In TAD, the cross-section of these structures is given by x_{sect1}, as it was for branches. A constant length of 1/3 of the grid cell width was estimated to represent the average petiole/twig length necessary to distribute the leaf blades uniformly within the entire grid cell. In the case of petioles that length seems unnaturally long relative to the area of a single leaf blade, if one thinks only of simple leaves on single petioles. However, to distribute leaf blades in a volume as large as the grid cells without twigs, natural trees would use some form of compound leaf. Thus one needs to include the long central rachis in the petiole length estimate, which makes the 1/3 estimate more reasonable. In nature there

are many intermediate strategies that use some combination of petioles and twigs, but this complication will not be considered in the current version of the TAD model. In TAD, seedlings either support their leaves using only twigs or only rachises, and this parameter is an independent trait.

3.4.2.4. Mechanical constraints. The inclusion of mechanical constraints on seedling growth in TAD is very important to producing realistic model tree seedlings. Simulations with a preliminary version of TAD that did not include mechanical constraints showed that without the need for mechanical support, the optimal stem design has a very small cross-section area with a few large diameter high conductivity vessels that are able to supply sufficient water for a relatively large crown. In nature this design is represented in the form of vines and lianas (Rowe and Speck, 2004). Since in our investigation, we are interested in free-standing self-supporting tree seedlings, we needed to include mechanical constraints in TAD. This preliminary model result illustrates how experimental studies of tree stems could benefit from studying the adaptation to hydraulic as well as mechanical requirements at the same time. A few experimental studies have started taking this holistic approach (Gartner, 1995).

3.4.2.4.1. Stem mechanics. A number of theoretical approaches to the mechanical analysis of tree trunks and plant stems have been used. Some adopt the critical buckling height for a column supporting its own weight (Niklas, 1994a, 1994b, 1999, 2004), which is a modified version of Euler's formula that in turn is known as Greenhill's formula (Greenhill, 1881). King modified this formula to include a crown weight that loads the column at a point that is located at 0.9 of the column height above the ground (King and Loucks, 1978; King, 1981, 1986). Other researchers have used Euler's formula to derive formulas for a self-loaded column bending under a horizontal force representing a wind load or a rope pulling in an experiment (Wood, 1995; Neild and Wood, 1999). Another simple approach when studying only the effect of wind loading is to approximate the stem as a cantilever beam under bending (Niklas, 2000), similar to the way that branch mechanics are analysed in TAD as described in the next section. All of these approaches were useful and appropriate for their application, but are not ideal for the TAD model. The ideal equation for TAD includes

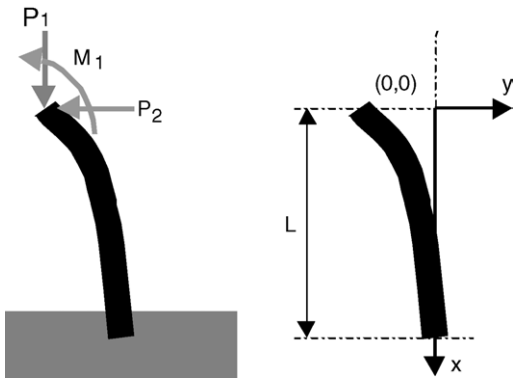

Fig. 5. Column under generalized bending loads. The distance x is positive in the downward direction from the origin labeled (0,0) in the right diagram to simplify the calculations. The distance y is positive in the direction to the right from the origin.

both vertical and horizontal forces applied at the top of a column as illustrated in Fig. 5. This more generalized solution is necessary to facilitate breaking the crown into segments connecting individual grid cells (as in Fig. 4). The vertical force in the figure can be thought of as representing the weight of the leaves and branches in the grid cell, and the horizontal force as the drag force from wind. We derived an analytical solution to calculate the factor of safety for this scenario. In our solution, we generalized the problem even further by also including a moment applied at the top of the column as well as the vertical (weight) and horizontal forces (wind) (see Fig. 5).

Equations for the reaction forces and moment may be derived by considering the deflection of the column (illustrated in Fig. 5) using the equation for an elastic curve (see Chapter 8 in Beer and Johnston, 1985), also known as the bending equation or Euler's equation (ca. 1774):

$$\frac{\partial^2 y}{\partial x^2} = \frac{M}{E_{\mathrm{MOE}} I_{\mathrm{MOI}}} \tag{40}$$

M is the moment applied, E_{MOE} is the modulus of elasticity, and I_{MOI} is the moment of inertia. In this case, the equation for the elastic curve becomes:

$$\frac{\partial^2 y}{\partial x^2} = \frac{-M_1 - P_1 y - P_2 x}{E_{\mathrm{MOE}} I_{\mathrm{MOI}}} \tag{41}$$

or

$$y'' + \frac{P_1}{E_{\mathrm{MOE}} I_{\mathrm{MOI}}} y = -\frac{P_2}{E_{\mathrm{MOE}} I_{\mathrm{MOI}}} x - \frac{M_1}{E_{\mathrm{MOE}} I_{\mathrm{MOI}}} \tag{42}$$

with the following end conditions, assuming that the base of the column is fixed:

$$y = 0, \quad \text{if } x = L$$
$$y' = 0, \quad \text{if } x = L$$

The solution to the preceding differential equation gives the deflection of the column:

$$y = A \sin(\omega x) + B \cos(\omega x) - \frac{M_1}{P_1} - \frac{P_2 x}{p_1} \tag{43}$$

where

$$A = \left(\frac{M_1}{P_1} + \frac{P_2 L}{P_1}\right) \sin(\omega L) + \left(\frac{P_2}{P_1}\right) \frac{\cos(\omega L)}{\omega}$$

$$B = \left(\frac{M_1}{P_1} + \frac{P_2 L}{P_1}\right) \cos(\omega L) - \left(\frac{P_2}{P_1}\right) \frac{\sin(\omega L)}{\omega}$$

$$\omega = \sqrt{\frac{P_1}{E_{\mathrm{MOE}} I_{\mathrm{MOI}}}}$$

Assuming a circular cross-section for the column with radius R, the moment of inertia can be calculated as follows:

$$I_{\mathrm{MOI}} = \frac{1}{4}\pi R^4 \tag{44}$$

The deflection of the column at the top ($y_{x=0}$) is obtained by letting $x = 0$ in the preceding equation. Now that the deflection of the column is known, it is possible to calculate the maximum stress in the column. The maximum stress will be at the base of the column and is the sum of the bending stress and the compressive stress from the vertical force:

$$\sigma_{\max} = \frac{M_{\mathrm{b}} R}{I_{\mathrm{MOI}}} + \frac{P_{\mathrm{b}}}{A_{\mathrm{b}}} \tag{45}$$

$$M_{\mathrm{b}} = M_1 + P_1 y_{x=0} + P_2 L \tag{46}$$

$$P_{\mathrm{b}} = P_1 \tag{47}$$

M_{b} and P_{b} are the reaction moment and reaction force at the base, respectively. A_{b} is the cross section area of the column, and R is its radius.

To calculate the factor of safety of the column against failure, the wood strength needs to be known. The strength of wood can be predicted fairly accurately from just its density using empirical relationships. The following relationships for green wood from the Wood Handbook (Forest Products Laboratory, 1999) were used in the model:

For softwoods:

$$E_{\mathrm{MOE}} = 1.61 \times 10^{10} G^{0.76} \tag{48}$$

$$\sigma_{\mathrm{comp}} = 4.97 \times 10^{7} G^{0.94} \tag{49}$$

For hardwoods:

$$E_{\mathrm{MOE}} = 1.39 \times 10^{10} G^{0.72} \tag{50}$$

$$\sigma_{\mathrm{comp}} = 4.90 \times 10^{7} G^{1.11} \tag{51}$$

The maximum compression stress (σ_{comp}) was chosen rather than the modulus of rupture (MOR) in bending because the combined maximum stress ($\sigma_{\max}$) is actually a compression stress and wood is much weaker in compression than under tension (Forest Products Laboratory, 1999). The reader may refer to Mattheck for a more detailed discussion of mechanical failure in trees (Mattheck et al., 1995; Mattheck, 1998). The mechanical factor of safety is then:

$$FS_{\mathrm{stem}} = \frac{\sigma_{\mathrm{comp}}}{\sigma_{\max}} \tag{52}$$

The factor of safety must be greater than one at all times if the column is not to break.

The preceding mechanical analysis cannot be applied to the whole stem in TAD, because the stem is not a single entity in the model representation but rather consists of a series of stem segments, each connecting two grid cells, as illustrated in Fig. 4. The mechanical analysis needs to be applied to each stem segment individually. As shown in the diagram the simplified architecture consists of vertical stem segments and horizontal branch segments.

Each segment must not only support the weight and wind forces on the leaves in its grid cell, but also the forces and moments from the stem and branch segments extending from it. This is the reason why it was necessary to derive the general case of a column subjected to horizontal and vertical forces as well as a moment at the top of the segment. The forces and moments for each segment are calculated as follows.

The vertical load, P_1 is the sum of the weights of the plant materials in the grid cell and all grid cells that it supports. The weight of the plant materials in a grid cell includes the dry weight of the stem/branch, twigs/petioles, and leaf blades, as well as the water that they contain. The horizontal load, P_2 consists of the wind load acting on the leaves and branches in its gird cell, plus the sum of the horizontal forces that act on the adjacent stem and branch segments that it supports. The moment load, M_1 is the sum of the reaction moments, M_b acting on the adjacent stem and branch segments that it supports.

The wind load acting on a grid cell is calculated as follows. For the relatively short saplings considered in TAD, wind speed can be approximated to vary linearly with height above ground as follows:

$$V_{\text{wind}} = 4 + 2\frac{H_{\text{gridcell}}}{30} \tag{53}$$

where V_{wind} is the wind speed, and H_{gridcell} (cm) is the height at the top of the grid cell. Thus, the wind speed at 300 cm above the ground would be 24 m/s (86.4 km/h), which is the maximum we have measured at a forest edge in southern Quebec in 2001. This wind speed is very high because the mechanical constraint should test if the seedling would break under the highest wind gusts to which it might be subjected. The drag force on a branch in the wind is calculated as follows (see Chapter 9 in Fox and McDonald, 1992):

$$F_{\text{D}} = \left(C_{\text{DL}}\frac{1}{2}A_{\text{leaf}} + C_{\text{DB}}A_{\text{branch}}\right)\frac{1}{2}\rho_{\text{air}}V_{\text{wind}}^2 \tag{54}$$

where C_{D} is the drag coefficient, A_{leaf} is the leaf area, and ρ_{air} is the density of air. Assuming standard air, the density of air is $\rho_{\text{air}} = 1.23\,\text{kg/m}^3$, and the viscosity is $\mu_{\text{air}} = 1.78 \times 10^{-5}\,\text{kg/(m s)}$. The Reynolds number for this flow is given by

$$Re = \frac{\rho_{\text{air}}V_{\text{wind}}D_{\text{leaf}}}{\mu_{\text{air}}} \tag{55}$$

The characteristic length for the flow is the leaf width, $D_{\text{leaf}} = 0.08$ m. Thus for $V_{\text{wind}} = 14$ m/s, the $Re = 77393$. Under such a large flow the leaf would bend and its effective area would be reduced. Therefore, the shape of the leaf is approximated by a hollow hemisphere and the area is assumed to be about half of the actual area of the leaf. The drag coefficient for a hemisphere is $C_{\text{DL}} = 0.38$ and $C_{\text{DB}} = 1.0$ for a cylindrical branch segment with $Re > 1000$ (Table 9.3 in Fox and McDonald, 1992), which is always the case for this application.

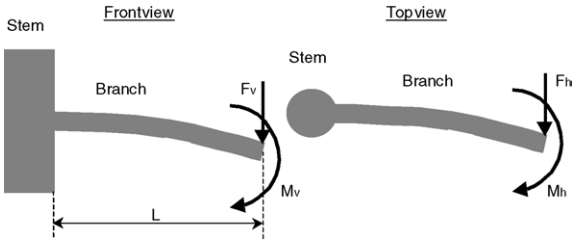

Fig. 6. Bending forces on branches.

3.4.2.4.2. Branch mechanics. For branches the wind and gravity loads are considered not to interact since they are orthogonal to each other (Fig. 6). The mechanical analysis is for a cantilever beam as follows (Chapter 4.4. in Beer and Johnston, 1985):

$$\sigma_{\text{v}} = \frac{\text{Mr}}{I_{\text{MOI}}} = \frac{4}{\pi R^3}(M_{\text{v}} + F_{\text{v}}L) \tag{56}$$

$$\sigma_{\text{h}} = \frac{\text{Mr}}{I_{\text{MOI}}} = \frac{4}{\pi R^3}(M_{\text{h}} + F_{\text{h}}L) \tag{57}$$

where M is the bending moment, R is the radius of a cylindrical branch segment, and I_{MOI} is its moment of inertia. The larger of the two stresses, σ_{v} and σ_{h} is then used as σ_{max} to compute the factor of safety using the maximum compressive stress as before for stems

$$FS_{\text{branch}} = \frac{\sigma_{\text{comp}}}{\sigma_{\text{max}}} \tag{58}$$

The forces and moments are calculated as follows. The vertical force, F_{v} is the sum of the weight of the seedling parts in the grid cell, and the vertical force of the neighboring branch segments that it supports. The horizontal force, F_{h}, is the sum of the wind force on the leaves in the grid cell, and the horizontal force of the supported neighboring branch segment. The bending moment in the vertical plane, M_{v} is the sum of the vertical force F_{v} multiplied by the length L, and the bending moment in the vertical plane of the supported neighboring branch segment. Similarly, the bending moment in the horizontal plane, M_{h} is the sum of the horizontal force F_{h} multiplied by the length L, and the bending moment in the horizontal plane of the supported neighboring branch segment.

3.4.2.4.3. Root anchorage. The study of root anchorage in tree seedlings has received much less attention than in adult trees, probably because windthrow is not a significant cause of mortality in juvenile trees. Nevertheless, it is not possible to fully understand the root systems of tree seedlings without taking anchorage into consideration. Even in tree seedlings the majority of root mass is contained in thick roots near the base of the stem to give mechanical stability, not in fine roots for nutrient uptake. Studies of tree seedling root systems are well served to combine both resource uptake and mechanical functions in modeling root form and function.

Several conceptual and analytical models for the analysis of the mechanics of root anchorage have been presented (Coutts, 1983; Ennos and Fitter, 1992; Ennos, 1993, 1994, 2000; Niklas, 1998; Mattheck, 1998). There are two aspects to root anchorage: the ability of the thick roots to withstand the mechanical stresses transferred to them from the stem, and the ability of the soil to resist these stresses when they are transferred from the roots. In seedlings, the ability of the roots at the base of the stem to withstand mechanical stresses is typically the weakest point. Therefore the model only considers this type of failure at the base of the stem. The failure of the soil itself (windthrow) is more typically a problem in large trees, particularly in trees with shallow root systems on weak soils.

In young trees, the root crown at the juncture with the stem base may break if it cannot support the bending moment transferred to this point. The bending moment could be supported by a single central taproot or by several large diagonal or lateral roots that come together at the root crown to form a single main root. The equations for the mechanical analysis of this main root are analogous to the analysis for branches as follows:

$$\sigma_{\text{root}} = \frac{\text{Mr}}{I_{\text{MOI}}} = \frac{4}{\pi R_{\text{taproot}}^3}(M_{\text{b}}) \tag{59}$$

where M_{b} is the moment at the base of the stem, and R_{taproot} is the radius of the main root at the base of the stem. The mechanical factor of safety is

$$FS_{\text{root}} = \frac{\sigma_{\text{comp}}}{\sigma_{\text{root}}} \tag{60}$$

The factor of safety is only calculated for the main root in the grid cell immediately below the base of the tree, since that is where the greatest stress occurs.

3.4.3. Fine roots (uptake of soil resources)

Because soil hydraulic conductance depends not only on soil properties but also on fine root density (i.e. root length per soil volume) we treat both topics together in this section. This section also includes the modeling of nutrient uptake, particularly active uptake, which depends on the level of fine root metabolic activity.

3.4.3.1. Soil hydraulic conductance. The soil conductance is computed from the specific soil conductance (ε) as follows:

$$C_{\text{s}} = \frac{s_{\text{root}}\ \rho x \varepsilon}{d} \tag{61}$$

where s_{root} is the root surface area, x is a constant converting the units from cm hydraulic head to MPa, and ρ is the density of water. The specific hydraulic conductance is a function of soil moisture as explained in the section on soil resources. The variable d is the distance the water must flow to the root, which is estimated from the root density (root length per soil volume):

$$d = \frac{1}{2}\left(\frac{V_{\text{gridcell}}}{R_{\text{L}}}\right)^{1/2} \tag{62}$$

The ratio of root length (R_{L}) to grid cell volume (V_{gridcell}) in the equation is known as the fine root density, which is of great importance for water and nutrient uptake as well as competition.

3.4.3.2. Nutrient uptake. Nutrient uptake has both a passive and an active component. The passive uptake is simply the product of water uptake and the nutrient concentration of the soil pore solution. The active uptake is modeled assuming Michaelis–Menten kinetics as follows:

$$\varphi = \frac{\varphi_{\max}(N_{\text{soil}} - N_{\text{soilmin}})}{k_{\text{nut}} + (N_{\text{soil}} - N_{\text{soilmin}})}\frac{\theta}{C}\frac{1}{d} \tag{63}$$

where N_{soil} and N_{soilmin} are the nitrate concentration in the soil solution and the minimum concentration necessary for uptake, respectively. θ is the soil water content, C is its water holding capacity, and k_{nut} is a Michaelis constant. This formulation implies that at low nitrate concentration uptake is limited by diffusion of nitrate to the root surface; whereas at high nitrate concentration the number of active uptake sites on the fine root surface limit uptake. The maximum rate of active nutrient

uptake (φ_{max}) is assumed to be a linear function of the fine root nitrogen content (R_N), a measure of metabolic activity:

$$\varphi_{max} = c_{nut}(R_N - 0.01) \quad (64)$$

3.4.3.3. Fine root tissue density, longevity, and diameter. Among ecophysiological traits, those of fine root traits are least well understood, which requires making simplifying assumptions in the current version of TAD. For example, root diameter is considered to be the most important factor governing longevity of thick roots in trees and shrubs (Gill and Jackson, 2000). However, this relationship is not supported for tree fine roots when comparing different species (Espeleta and Donovan, 2002). Therefore a constant fine root diameter of 0.05 cm (Comas and Eissenstat, 2004 and our unpublished data) and constant longevity of 30 weeks were assumed (Eissenstat, 1991; Eissenstat et al., 2000; Wells and Eissenstat, 2001; Wells et al., 2002). Similarly, the tradeoffs associated with fine-root-tissue density in trees are currently still poorly understood (Eissenstat and Yanai, 1997). Consequently fine-root-tissue density was conservatively assumed to be the same as the wood density for thick roots, since fine roots need to withstand the same low water potentials as the thick roots. We consider these approximations for fine root traits to be very coarse and consequently are an inevitable source of inaccuracy in TAD as they are in other tree models. In our view this lack of a better understanding highlights the urgent need to focus greater effort on fine root traits in ecophysiology research.

3.5. Tissue construction costs

The carbon costs for the construction of a tissue are a function of the volume of tissue, its density, and the cost of synthesizing a unit mass of the tissue. The construction cost for woody tissues (fine roots, thick roots, stems and branches) is:

$$\alpha_{wood} = \rho_x \xi \zeta V_{wood} \quad (65)$$

where ρ_x is the density of xylem wood, ξ the cost of tissue synthesis, ζ the carbon content of the tissue, and V_{wood} is the volume of wood.

Leaf blades may be supported by rachi in the case of compound leaves or by woody twigs in the case of simple leaves as explained earlier. The construction cost for twigs is calculated in the same way as for woody tissues, but for rachi the cost should be less, since they are a less durable and less lignified structure. By comparing the construction cost for twigs bearing the simple leaves of *Ulmus rubra* to the rachises bearing leaflets of the compound leaves of *Juglans nigra*, Givnish (1995) found that the construction costs of twigs were about 1.5 times as much as for rachises. Therefore, in the TAD model rachises are assumed to have 0.667 times the construction cost of twigs.

To calculate the construction cost of leaf blades in TAD, we assumed that on a mass basis the construction cost is the same for cell walls, sclerenchyma and cuticles:

$$\alpha_{leaf} = \rho_{cellwall} \xi \zeta (V_{cellwall} + V_{schl} + V_{cuticle}) \quad (66)$$

where, $\rho_{cellwall}$ is the density of cell wall tissue, and the V's are the respective volumes of each tissue type.

3.6. Resource balances

The resource balances considered in the TAD model are the following, in order: (1) water, (2) carbon, and (3) nitrogen.

3.6.1. Water balance calculations

The water balance calculations in the TAD model are of great importance because they are at the center of how the state of the model is updated from one time step to the next. The model assumes that the water transported into the leaves in a grid cell equals the water transpired by those leaves. In other words transient effects related to water storage in leaves or stems are neglected. This assumption is reasonable in tree seedlings since they have a relatively small stem volume (i.e. little water storage capacity) and the path of water conductance is short. The water transpired by the leaf per time step is controlled by the stomatal conductance as described earlier in the section on leaf gas exchange. The water uptake matching the leaf transpiration is driven by the gradients in water potentials in the plant and the soil. The water potentials required for this flow are computed using an Ohm's law analogy where the hydraulic conductances are represented like a network of electrical resistors (Tyree and Ewers, 1991) as illustrated in Fig. 7.

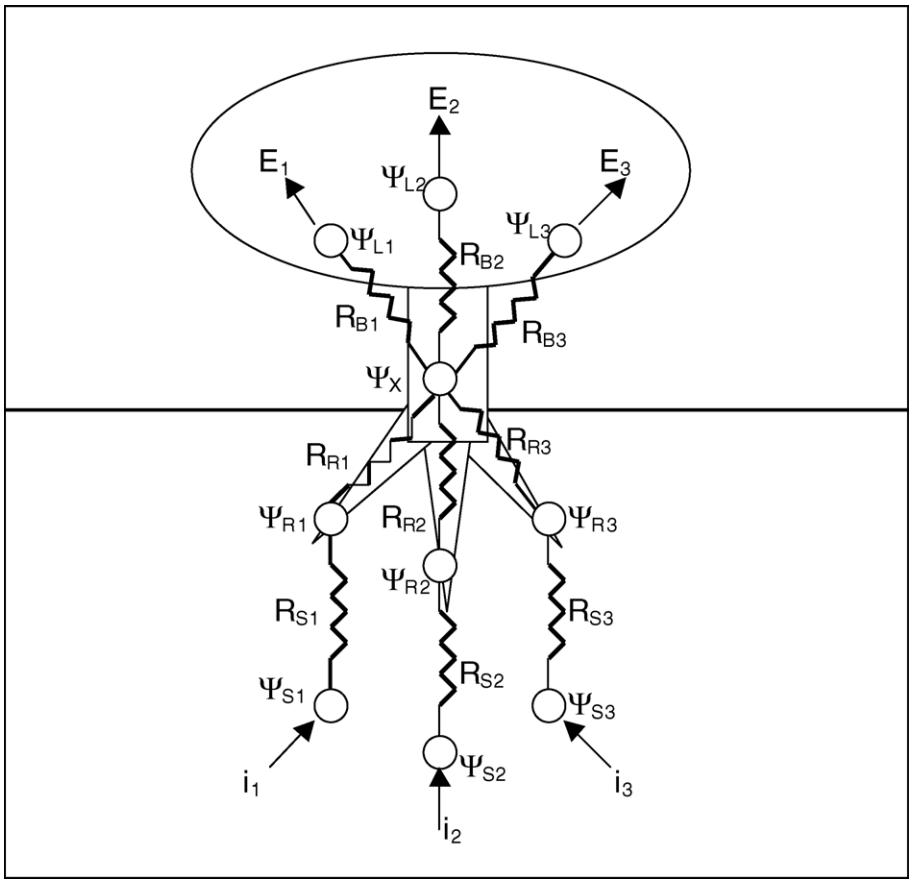

Fig. 7. Schematic illustration of hydraulic resistance network of a seedling in analogy to an electrical circuit. The R's are the resistances, Ψ's the water potentials, E's the transpiration fluxes, and i's are the water uptake fluxes. In this example, the seedling occupies three below ground grid cells, and three above ground grid cells (grid cell divisions are not drawn to avoid clutter), but the equations derived below are valid for any number of grid cells.

In this approach, the water potentials in the plant are a function of the fluxes and resistances, which neglects any effects of gravity on water potential. This assumption is reasonable for the seedlings simulated in the model, but would not apply in very tall trees. According to Ohm's law the flux of water taken up by a root may be calculated as:

$$i_n = \frac{(\Psi_{Sn} - \Psi_x)}{(R_{Rn} + R_{Sn})} \tag{67}$$

where n is the number of the grid cell. According to Kirchoff's laws of circuit analysis, the sum of the water uptake fluxes, $\sum i_n$ must equal the sum of the water-transpired fluxes, $\sum E_n$. Therefore, it can be shown that the water potential of the xylem, Ψ_x is equal to the following:

$$\Psi_x = \frac{\sum_n [\Psi_{Sn}/(R_{Rn} + R_{Sn})] - \sum_n E_n}{\sum_n [1/(R_{Rn} + R_{Sn})]} \tag{68}$$

Once the xylem water potential (Ψ_x) is known it is possible to calculate the root (Ψ_{Rn}) and leaf (Ψ_{Ln}) water potentials as follows:

$$\Psi_{Rn} = R_{Rn} i_n = \Psi_x \left(1 - \frac{R_{Rn}}{R_{Rn} + R_{Sn}}\right) + \Psi_{Sn} \left(\frac{R_{Rn}}{R_{Rn} + R_{Sn}}\right) \tag{69}$$

$$\Psi_{Ln} = \Psi_x - R_{Ln} E_n \quad (70)$$

Thus, if the total seedling transpiration is known these three equations can be used to compute the water potentials in the seedling from the water potentials of the soil grid cells in the previous time step. The transpiration rates are calculated as described in the section on leaf gas exchange. Resistance is simply the inverse of conductance.

The calculated leaf water potential is compared to the minimum allowable leaf water potential, which is a function of the osmotic potential. If the calculated leaf water potential drops below the allowable minimum, then the leaves in the grid cell wilt. If leaves have wilted, the model program sets the leaf area of the affected plant to zero in that grid cell. Similarly the root (Ψ_R) and stem (Ψ_x) water potentials are compared to the allowable minimum, the potential at which catastrophic xylem cavitation is initiated. If root water potential drops below the threshold, the model program sets the fine root length of the affected seedling to zero in that grid cell. However, if catastrophic xylem cavitation is initiated in the stem, then the whole plant is considered to have wilted and the seedling dies. Thus the stomatal control parameters (c_1 and c_2 in the section on leaf gas exchange) need to limit transpiration sufficiently to prevent such drought-induced mortality.

Once the water balances have been calculated for each seedling, the total water uptake from each soil grid cell can be computed by summing the water uptake of all the individual seedlings rooted in that grid cell. This uptake is subtracted from the water in the soil grid cell. Time steps for the water balance calculations were set sufficiently small to prevent this uptake from ever exceeding the water availability during the simulations. The water present in the soil after the water uptake is subtracted is used to obtain the soil water potential (Ψ_S) for the water balance calculations in the next time step. This feedback on soil water potential affects the accuracy of the simulation. In nature, the soil water potential adjusts continuously as water is taken up, while in the model it adjusts only at the end of each time step. Thus, the smaller the time step the more accurate the simulation, but also the longer it takes for a simulation to run. In the simulations a time step of 3 h was sufficiently small to avoid numerical instabilities and to obtain sufficiently accurate results.

Another potential problem with numerical water balance calculations is in the special case when a seedling extends its root to a deeper soil grid cell that is moister than the grid cells that its roots already occupy. The new roots establish a hydraulic connection between the soil grid cells, which allows flow from a moist grid cell to a drier grid cell through the root system. In nature this phenomenon occurs in adult trees of some species with large deep root systems and is called hydraulic lift (Caldwell and Richards, 1989; Dawson, 1993; Burgess et al., 1998). The reverse process of water redistributed from moist surface layers to drier deep soil layers has also been demonstrated (Schulze et al., 1998; Burgess et al., 2001). However, the discrete nature of the TAD model causes the connection to appear very suddenly, which can create numerical instability. Therefore the model code does not allow any reverse flows (i.e. flow out of the roots into the soil). Preventing hydraulic lift in the model should not be a serious issue since hydraulic lift has never been demonstrated to be important in seedlings.

3.6.2. Carbon balance calculations

Carbon is taken up through photosynthesis and lost through respiration. Any surplus from the balance of these processes is available for growth or storage. If the balance is negative and stored carbon reserves have been depleted, the seedling dies.

The carbon uptake is simply the realized photosynthetic rate multiplied by the length of the time step. The photosynthetic rate is a function of the leaf traits, the stomatal conductance, the incident light, and the atmospheric CO_2 concentration as explained in detail earlier. The stomatal control is a compromise between increasing the carbon uptake and preventing wilting and xylem cavitation.

The seedling respiration or carbon loss is the product of the maintenance respiration rate and the time step. Maintenance respiration rate is taken to be a linear function of tissue nitrogen content, assuming that nitrogen content is representative of enzyme content and thus metabolic activity. The empirical data from Reich et al. (1998a,b) was used to approximate a general relationship between maintenance respiration rate and tissue nitrogen content

$$M_{RESP} = (B_R R_N + B_{TR} X_N + B_S X_N + B_L L_N)\, m_{resp} \quad (71)$$

where B_R, B_{TR}, B_S, and B_L are the respective mass of carbon in fine roots, thick roots, stems and branches, and leaves. R_N, X_N, and L_N are the respective nitrogen concentrations in fine roots, xylem or wood, and leaves. Note that for roots this rate includes the respiration for active nutrient uptake indirectly through the increased nitrogen content associated with higher active uptake (see Section 3.4.3).

If surplus carbon is not used in growth, it may be stored. Storing carbon can be advantageous in a stochastic or seasonal environment where stored carbon can be used to cover maintenance respiration costs during adverse periods such as drought or winter. The carbon storage capacity is limited by the size of the seedling. We set the storage capacity in g carbon to 20% of the dry mass in roots (fine roots + thick roots) plus 10% of the dry mass in shoots (leaves + branches + stem). These limits are based on measurements reported in several studies (Loescher et al., 1990; page 168 in Kozlowski and Pallardy, 1997; Hoch et al., 2003; Körner, 2003). The conversion and translocation of carbohydrates associated with this long-term storage has a cost. To account for this cost the amount of carbon moved into storage was reduced by 10%.

Interestingly, preliminary simulations run prior to limiting the storage capacity yielded tree seedling designs with very unrealistic growth patterns. Introduction of the carbon storage constraint in the TAD model eliminated this unrealistic behavior, implying that this constraint likely also has an important influence on the evolution of tree form and behavior in nature. Consistent with this hypothesis, experimental studies have also shown that in trees, especially in canopy trees, the carbon storage can be limited more by storage capacity and translocation rates than by carbon supply (Körner, 2003).

3.6.3. Nitrogen balance calculations

Nitrate status does not have any direct effect on survival, acting only indirectly through its effect on growth and consequently on carbon balance. Nitrogen is needed for growth. The effect of nitrate on growth depends on its availability relative to the availability of carbon and the relative amounts of nitrogen to carbon needed for construction of different tissues. Thus the nitrogen content of different tissues and the type of environment are key to determining the effect of nitrate. Surplus nitrogen can be stored like surplus carbon, but unlike carbon the nitrate storage capacity of seedlings was not limited in the TAD model, since surpluses of nitrate were always relatively small.

3.7. Mortality

Several types of mortality can occur in the model. Drought (see Section 3.6.1), mechanical failure (see Section 3.4.2.4.1), and carbon starvation (see Section 3.6.2) can all cause seedling mortality. Although mechanical failure of stems or root anchorage is not always fatal in nature, in the model it is treated as being fatal since it is presumed to put the seedling at too great a competitive disadvantage on average.

As in nature, survival is the first fitness criterion in the model, mechanical integrity is the second, and growth is only the third. Thus fitness is computed as follows:

$$\text{Fitness} = \frac{B_{\text{total}}}{t_{\text{sim}}} \tag{72}$$

where t_{sim} is the number of days that the growth of the seedling design was simulated, and B_{total} is the total dry mass of the seedling at the end of the simulation if the seedling survived and did not fail mechanically, otherwise B_{total} is zero.

3.8. Allocation of available resources (nitrogen and carbon)

Carbon is allocated either to growth or to a storage reserve for later use. The carbon and nitrogen allocated to growth are further divided into above or below ground. The allocation coefficients are a function of time (t) according to a power law of the following form:

$$\text{Allo}_m = a_m + b_m(t)^{c_m} \quad \text{for storage,} \tag{73}$$

$$\text{Allo}_C = a_C + b_C(t)^{c_C} \quad \text{for carbon, and} \tag{74}$$

$$\text{Allo}_N = a_N + b_N(t)^{c_N} \quad \text{for nitrogen} \tag{75}$$

Although there is no direct experimental evidence that plants use such allocation rules, this approach has frequently been used successfully in plant growth models (for reviews see Nikinmaa, 1992; Jackson et al., 2001). Power laws were chosen because they are commonly used to scale with size/age in biology.

3.9. Growth

After survival has been insured the surplus in resources can be expended on growth according to the allocation rules explained in the previous section and the independent growth parameters explained in this section. Since the distributions of roots and leaves are explicit (between grid cells, but not within grid cells), a set of rules is necessary to determine where new growth is to occur. All growth occurs in cells already occupied until threshold intensity is reached. By threshold intensity a leaf area per grid cell (L_{int}) or a fine root length per grid cell (R_{int}) is meant. This threshold is a function of the resource availability as described by the following equations. Soil depth (d_{depth}) was used to modify root intensity since it is closely correlated with distribution of soil resources (nutrients and water). Tree root intensity has been shown to be correlated with soil nutrients in the field (Thomas, 2000).

$$L_{\text{int}} = S_{\text{grid}} L_{\max} I_{\text{level}} \tag{76}$$

$$R_{\text{int}} = R_{\max} V_{\text{cell}} \left(\frac{d_{\text{depth}}}{d_{\text{grid}}} \right)^{\delta} \tag{77}$$

where $L_{\max}$ and $R_{\max}$ are independent parameters specifying the relative maximum intensities. I_{level} is the relative light intensity, and d_{grid} is the maximum depth of the soil grid. If the threshold intensity is reached in all the occupied cells, then extension growth occurs into grid cells adjacent to the cells already occupied by the plant. A maximum crown width ($w_{\max}$), maximum root system width ($\text{wr}_{\max}$), and maximum rooting depth ($d_{\max}$) restrict this extension growth. These are independent traits that control the shape and extent of crown and root systems. There is no maximum height in the model at the moment since simulation times are too short for saplings to outgrow the grid used in simulations.

The growth of leaves is linked to growth in supporting stems and branches by the independent ratio x_{sect1}. This ratio insures that there is a minimum amount of xylem per leaf area. Similarly the independent ratio x_{sect2} links the growth of new fine roots to the amount of supporting thick roots.

In real plants, growth is reduced under drought stress because turgor is insufficient for cell expansion (Bressan, 1998). In the TAD model, a threshold that the average nocturnal leaf turgor pressure must exceed for shoot growth to occur includes this effect. This threshold was set to 0.7 MPa assuming that turgor for shoot extension needs to be slightly greater in woody plants than in the sunflower data given by Bressan (1998) due to their stiffer cell walls. The leaf turgor pressure ($T_{\text{L}n}$) is calculated as follows for each grid cell in the crown:

$$T_{\text{L}n} = \Psi_{\text{L}n} - \text{osm} \tag{78}$$

The calculation of growth is the final fitness measure assuming the constraints of survival and mechanical integrity are met. Thus with this fitness measure defined we are able to search for optimal tree seedling designs in the trait space defined by the model.

3.10. Genetic algorithm and model implementation

Goldberg (1989) and Mitchell (1996) provide thorough introductions to genetic algorithms, including advice on their application to different types of optimization problems. We used a GA with the standard features and parameter settings as recommended in Goldberg (1989) for maximum mathematical efficiency. The programming of the genetic algorithm and the seedling simulation model were implemented in the C language.

The genetic algorithm in TAD needs 1000–1500 generations to stabilize on an optimal solution, which takes about half a day to 3 days on a 1.6 GHz computer processor depending on the type of environment simulated. Thus the application of the current version of the TAD model is not restricted by computer speed. However, a future version that might simulate the entire life of a tree would need to wait until computers are at least 100 times faster.

4. Simulation

The genetic algorithm in TAD was run for 2000 generations to guarantee that the algorithm had stabilized on an optimal solution. We refer to the combination of trait values comprising this optimal solution at the end of the 2000 generations as an optimal design. Since such optimal solutions are locally stable, this combination of trait values could also be referred to as an evolutionary stable strategy or ESS (Maynard Smith, 1982), but since most of the independent traits that are

optimized in TAD are morphological or physiological rather than behavioral we prefer to call this optimal solution an optimal design.

Although the eventual purpose of TAD is to compare the optimal designs for different environments, here our purpose is the presentation of the TAD model and its realism. To demonstrate this realism we will present in detail the traits, behavior, and growth patterns for an example of an optimal tree seedling design found with TAD for a particular environment.

The tree seedling design presented here was optimized for average growth rate over 350 days while at the same time ensuring survival and mechanical stability in an environment that included competing neighbors. This environment had a loam soil, moderately humid air, high light, and a warm climate (Table 1). Soil water was replenished to 95% of field capacity in the topsoil layer every 15 days, in the second layer every 30 days, in the third layer every 45 days, and so on for the lower soil layers. The nitrate input to the soil was at a rate of 20 gN/m^2/year (typical of a fertile temperate forest site, Larcher, 2003), and the atmospheric CO_2 concentration was 375 ppm. Thus the environmental conditions for this first demonstration of the model could be thought of as a productive but dry environment such as an old field or a large forest gap during summer in a in a warm temperate region or in the tropics.

We also imposed a drought from day 90 to 150 of the simulation, since tree seedlings need to be able to withstand droughts even in relatively humid environments. We consider inclusion of at least one drought period relatively early in the seedlings life important since preliminary simulations showed that its inclusion improved the realism of seedlings. Although the precise environmental conditions we chose might seem arbitrary, other environmental conditions also produced realistic seedlings, and we will explore the effects of environmental differences in subsequent articles. Here we are primarily concerned with describing the TAD model and demonstrating the realism of the optimal seedling designs that emerge in a typical, intermediate test environment, by presenting an example of an optimal design.

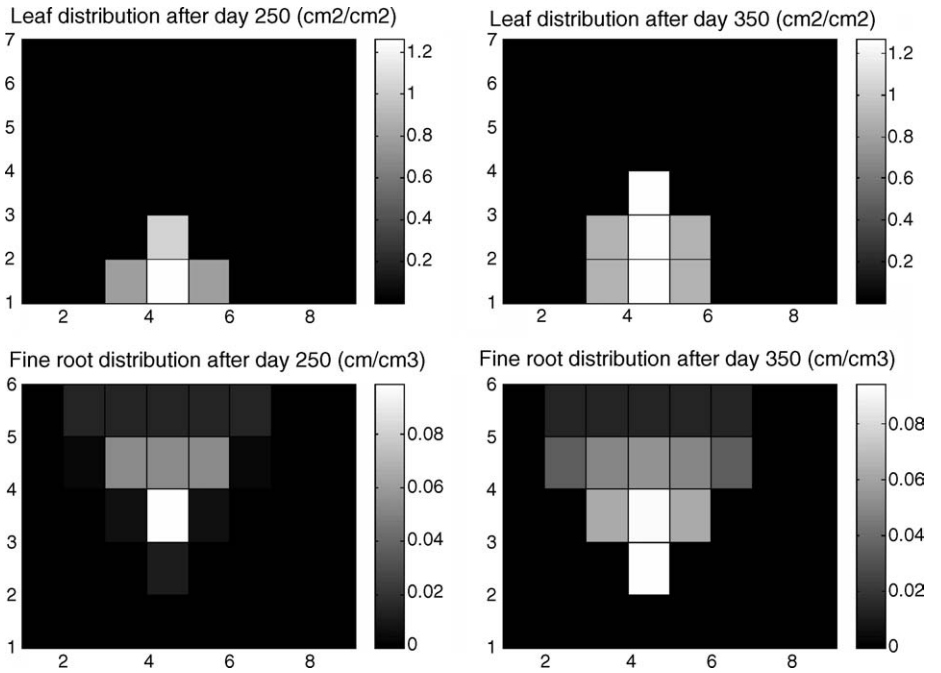

Fig. 8. The distribution of leaf area (top panels) and fine root length (bottom panels) for one of the tree seedlings within the vertical cross section grid above ground (top panels) and below ground (bottom panels). The competing neighbors are not shown for clarity since crowns and root systems overlap.

5. Results

The growth and resource uptake for the optimal tree seedling design found with the genetic algorithm in TAD is illustrated in Figs. 8–14. These figures are focused on the temporal patterns over the 350 day simulated growth period. Table A4 in Appendix A lists the values for a number of functional traits for this optimal model tree seedling. The range of values for these traits in natural tree seedlings is also listed for comparison. The listed traits were chosen because ecophysiologists frequently measure them and data for natural tree seedlings of a range of species were readily available.

6. Discussion and conclusions

The TAD model was derived using the holistic optimization approach advocated in Section 1. This approach gave priority to the interactions among organ level traits performing multiple functions at the whole plant level, rather than on all the details of individual functions. Despite the inevitable simplifications associated with this approach the optimal tree seedling design found by the GA for the particular environmental conditions is remarkably realistic. This model seedling can be examined at multiple scales of biological organization, from the overall pattern of growth for the whole seedling, to the variation in resource uptake by individual organs causing this overall pattern, to the diurnal dynamics of the exchange of resources of an individual organ, to the values of individual traits. We will examine the realism of the model seedling at each of these scales in turn.

The overall pattern of growth of the model tree seedling in our test environment showed a tendency to grow predominantly below ground during the first half of the simulated growth period, but then switched to predominantly growing above ground (Fig. 8). This behavior of an initial emphasis on root growth is observed in many natural tree species (Ledig et al., 1976), and is particularly pronounced in drought-adapted tree species such as those from the genera *Quercus* and *Carya* (Toumey, 1929; Holch, 1931; Biswell, 1935). Laterally, this design involved

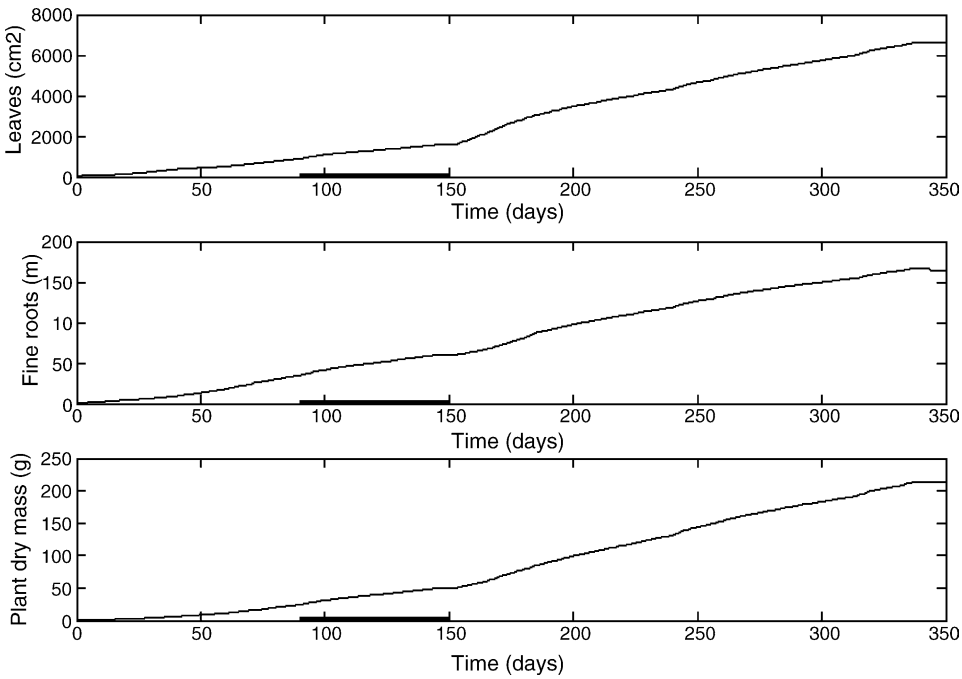

Fig. 9. Plots of total dry mass, leaf area and fine root length vs. time to illustrate the growth of the tree seedling. Note that the drought period was imposed from day 90 to 150, as indicated by the thick black line.

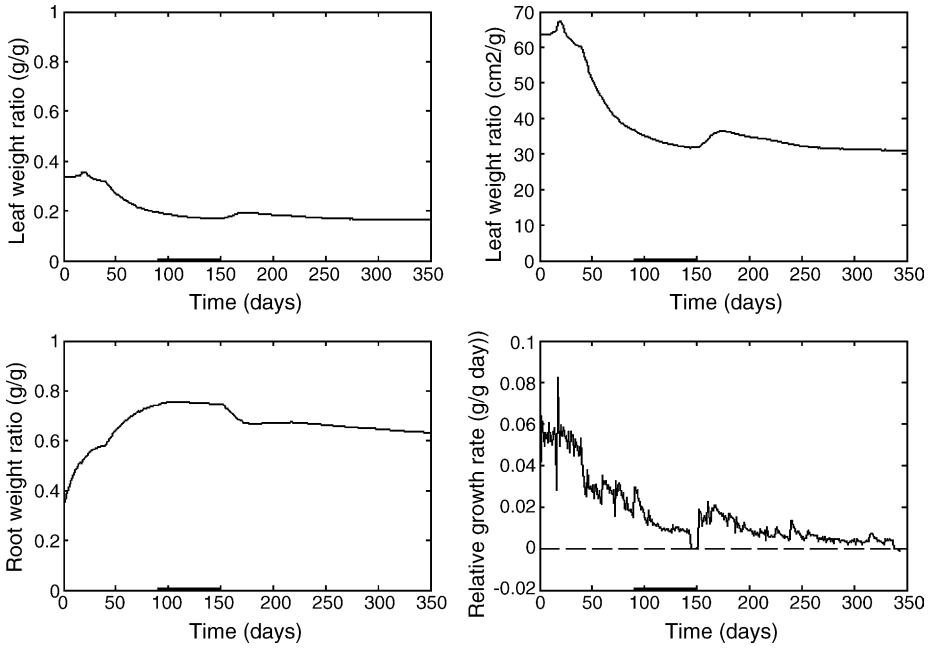

Fig. 10. Growth analysis of the seedling showing how leaf weight ratio, root weight ratio, leaf area ratio, and relative growth rate change with time in a correlated manner. The leaf weight ratio is defined as the fraction of plant dry mass that is leaves, and similarly the root weight ratio is defined as the fraction of plant dry mass that is roots. The leaf area ratio is defined as the total leaf area divide by the total plant dry mass. The relative growth rate is the growth rate of the plant relative to its size. (Lambers and Poorter, 2004) The thick solid line at the bottom of the figures indicates the drought period.

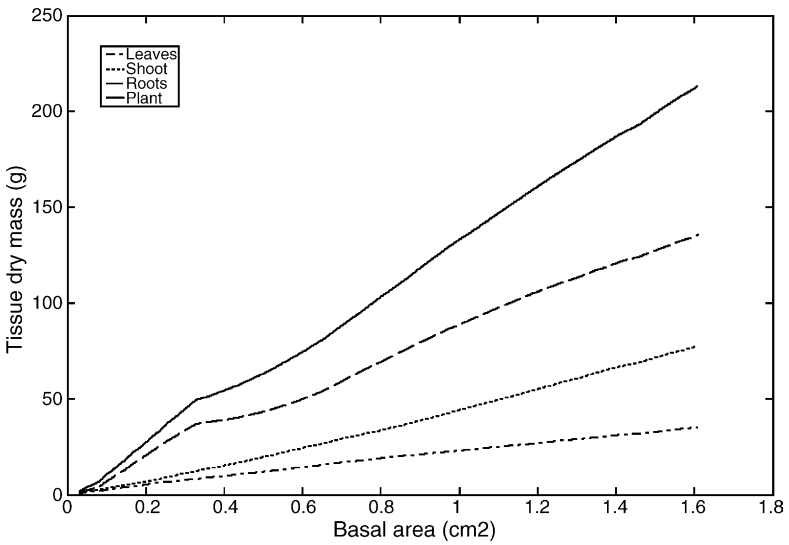

Fig. 11. An allometric representation of the seedling's growth.

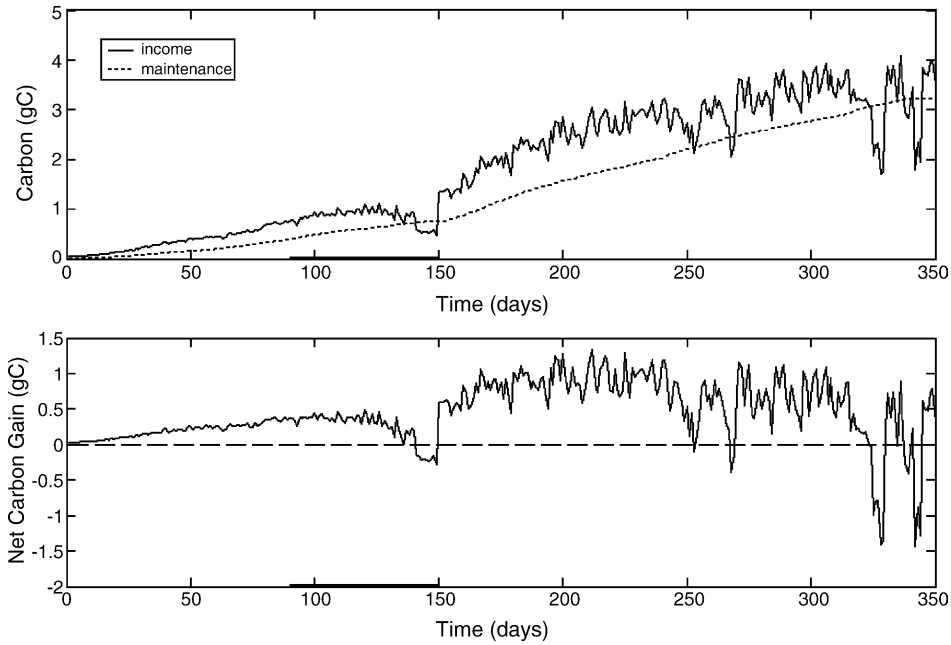

Fig. 12. The net carbon gain of the seedling plotted vs. time. Net carbon gain is the difference between carbon income and carbon expended for maintenance. The thick solid line at the bottom of the figures indicates the drought period.

extending roots farther than branches (Fig. 8). Consequently there is greater overlap between neighboring seedlings in roots than in crowns. This relatively low degree of crown overlap is presumably to avoid shading by neighbors. Natural tree seedlings usually also avoid growing into each other's crowns (our unpublished data), whereas, their root systems often show large overlap (Stout, 1956; and our unpublished data).

Extensive model validations with preliminary simulations under a range of environmental conditions (cf. Table 1) revealed that the growth curves for the diverse designs that emerge consistently have several growth phases; these phases are less pronounced for the design presented here (cf. Fig. 2) than for some other designs from our preliminary simulations. The seedling growth curve typically starts with an initial exponential phase, which implies a constant relative growth rate (RGR) as illustrated for the first 50 days in Fig. 10. In the following period the growth curve becomes nearly linear and RGR gradually declines as the increasing size of the seedling steadily increases support costs on a leaf area basis (Weiner, 2004) and competition by neighbors begins to have an effect. This ontogenetic shift is also observed in natural tree seedlings (Evans, 1972; Ledig et al., 1976) and it is a strength of the TAD model that this ontogenetic effect is faithfully reproduced (Körner, 1991).

In our example here, a drop in RGR from day 90 to 150 due to the imposed drought period interrupts the prolonged linear phase, but the previous trajectory is quickly resumed after day 150. Such drought-induced suppression of tree growth also is well known (Kozlowski and Pallardy, 1997). At the very end of the growth period, there is a phase where growth rate declines further due to intense crowding from the neighboring tree seedlings. At this point natural tree seedlings would begin the process of self-thinning (White, 1981; Westoby, 1984). That the model seedlings show this important turning point is a further indication of the model's realism.

These changes in growth rate with increasing seedling size present a challenge for experimental researchers who need a consistent basis for making comparisons among individuals or species (Coleman et al., 1994). One solution is to use relative growth rate (RGR) where growth rate is normalized by the size of the plant; RGR is the basic measure used in most modern growth analyses (Evans, 1972; Lambers and

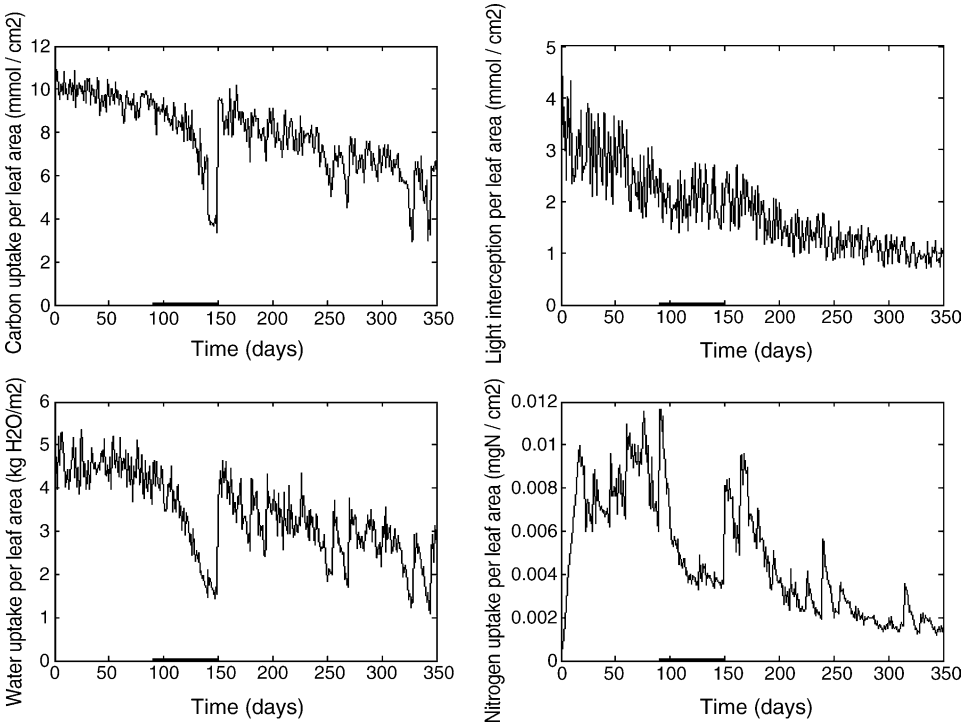

Fig. 13. Time series plots of the uptake of the four modeled resources: carbon, light, water, and nitrogen. The thick solid line at the bottom of the figures indicates the drought period.

Poorter, 2004). Comparative studies have discovered that RGR is most closely related to the leaf area ratio (LAR) (Körner, 1991; Lambers and Poorter, 2004). The model seedling's RGR also has a close relationship with LAR as shown in the right panels of Fig. 10. The leaf and root weight ratios (LWR and RWR, respectively) are other commonly used measures in growth analysis. The LWR and RWR plotted in the left panels of Fig. 10 illustrate shifts in allocation during different phases of the seedling's growth. Initially the emphasis is on root growth as mentioned previously and the RWR increases dramatically up to the beginning of the drought. After the drought, growth switches to predominantly shoot growth and RWR declines gradually. The LWR generally follows the opposite trend except near the end of the simulated growth period where LWR also declines gradually. During this final phase the seedling can no longer expand the size of its crown due to crowding from its neighbors and consequently shoot growth consists mainly of height rather than leaf area growth. The model seedling's values for RWR were higher than for natural tree seedlings from tropical montane forest (Lambers and Poorter, 2004), but not unreasonable considering that the simulated environment was relatively dry. The values for the LAR, LWR, and RGR compare well with values for natural tree seedlings (Lambers and Poorter, 2004).

An alternative approach to the problem of comparisons across ontogenetically diverse groups is to use an allometric framework where comparisons are made on a size basis rather than a time basis (Coleman et al., 1994; Weiner, 2004; Preston and Ackerly, 2004). The allometric relationships in the model seedlings (cf. Fig. 11) show the same kind of constancy as in natural tree seedlings (Körner, 1991; Weiner, 2004). This constancy is not programmed into the TAD model with an allometric equation, but rather is the outcome of the interaction among the independent allocation traits and the indirect effects of the other independent traits. Like the other results presented here, the allometric relationships are emergent patterns, and as such are a much stronger test of the model's overall realism than an

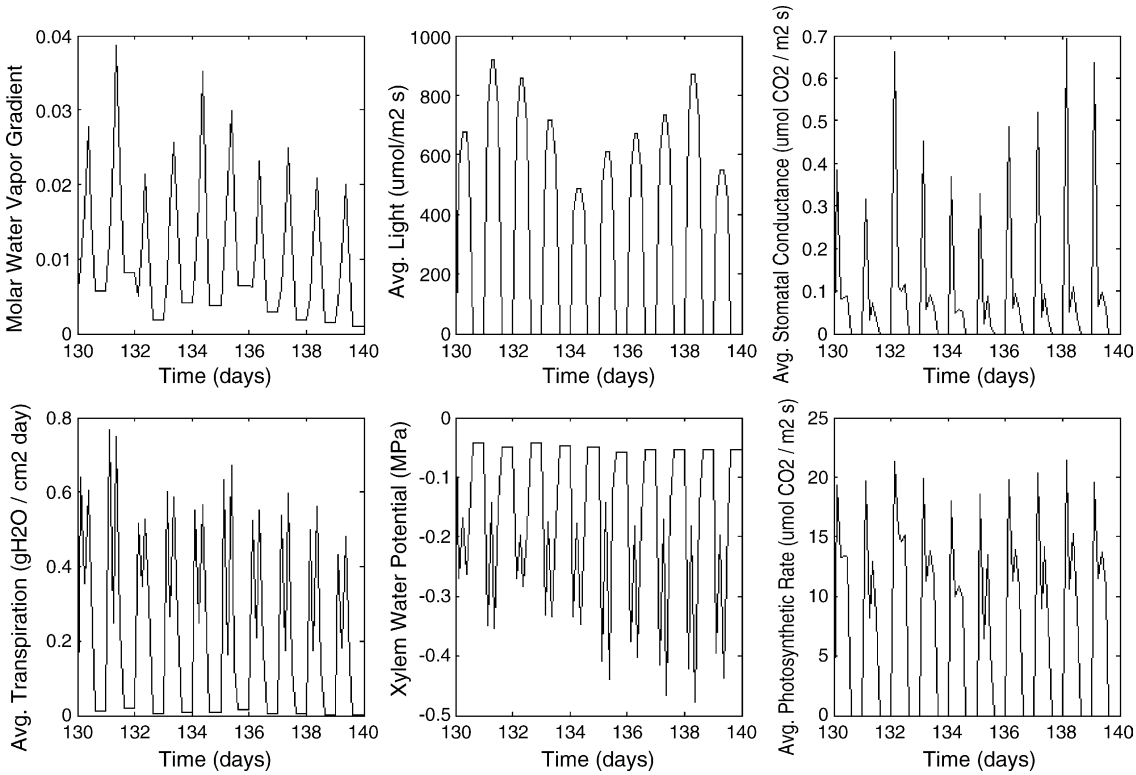

Fig. 14. Plot of a 10-day excerpt of the leaf gas exchange data including water vapor gradient from leaf to air, light intensity, stomatal conductance, transpiration rate, xylem water potential, and photosynthetic rate averaged over the all of the seedlings leaves. The first of the two upper panels represent environmental conditions that influence the response variables plotted in the other four panels. Note that these days fall within the drought event, and that water supply is diminishing steadily through the period.

examination of any individual model component would be.

Beyond the comparison of the overall growth pattern of the model seedling, the underlying causes of this variation in growth rate are also realistic. The underlying causes of the variation in growth rate can be examined by comparing the growth curves with the curves of resource uptake. In the model results, the growth curves run parallel to the curves for carbon income and maintenance costs (compare Figs. 9 and 12), although the income curve is much more irregular showing several prominent dips. The most prominent of these is at the end of the drought indicating that soil moisture may be an important factor in limiting carbon gain. This interpretation is reinforced by the resource uptake patterns (Fig. 13). In the two left panels of Fig. 13, carbon uptake per leaf area clearly shows the same pattern of dips as the water uptake per leaf area. Uptake of water and carbon are linked via the stomatal conductance implying that stomatal regulation is the controlling factor (Cowan and Farquhar, 1977). The continued decline in resource uptake per leaf area even after the drought ends suggests that the stomatal conductance is not only reacting to soil moisture. Stomata also react to light (Cowan and Farquhar, 1977), implying that the long decline in average light interception per leaf area due to self-shading and neighbor-shading with increasing size is the ultimate reason for the decline in carbon uptake and therefore also growth rate. Given that a large proportion of the nitrogen uptake was passive (69%) under the very fertile conditions in this simulation, we can expect that the nitrate uptake should largely decline in parallel to the water uptake as shown in the lower panels of Fig. 13. These strong, interacting effects of light and water availability on carbon uptake are also observed in nature (Kozlowski and Pallardy, 1997).

At an even finer scale than the causes of variation in growth rate, the diurnal leaf gas exchange patterns can also be investigated for realism. The stomatal control behavior is examined more closely in Fig. 14, where an excerpt of leaf gas exchange averaged over the crown is plotted for 10 days during the height of the drought period. These curves show that in response to the peaks in molar vapor gradient in the early afternoon, stomatal conductance is reduced greatly to reduce transpirational losses. Consequently the transpiration rate shows a sharp dip in midday that is typically also seen in real trees (Tenhunen et al., 1987; and our unpublished data). This midday dip is expected theoretically when water-use-efficiency is optimized on a diurnal basis (Cowan and Farquhar, 1977). Another consequence of this optimal behavior is that maximum photosynthetic rate occurs in the mornings (see Fig. 14), a fact that is well known to ecophysiologists (Pearcy, 1989).

Even though the priority of the model was on realism at the scale of the whole seedling rather than on realism in individual traits, it is noteworthy that even at the scale of the individual traits the model results are realistic. Specifically, of the 19 commonly measured ecophysiological traits listed in Table A4, only three of the values for the model seedling design fell outside the natural range, and even these were not unreasonable values. Given the simplifications and coarse approximations that were necessary in designing the TAD model, the high concordance with the natural values of traits is satisfying.

We conclude that overall the simulated seedlings not only look and behave realistically in the test environment, but also have reasonably accurate values for individual traits. Similarly realistic results have been found in our ongoing simulations in a wide variety of test environments. The accuracy of seedling trait values and the realistic responses observed in our simulations support the validity and utility of the approach taken in the TAD model. The notable strength of the TAD model lies in the fact that the values of traits and the nature of key functional responses are emergent properties, not the outcome of simple empirical rules programmed into the model. The outcomes observed result from the optimal resolution of tradeoffs among many conflicting functions contributing to seedling fitness. An important consequence of moving towards a more holistic approach is that the many interacting traits begin to behave as a complex system. Analyses of complex systems are providing many new insights of fundamental importance to biology and are attracting many modelers to problems in biological complexity (Proulx et al., 2005; Ellis, 2005). The TAD model is the first model of plant function that allows studying the interactions among traits as a complex system. Consequently, the TAD model is well suited to provide original insights into the general laws governing tree seedling design and trait evolution that go beyond conventional models in fundamental ways (Sutherland, 2005). For example, the modeling approach taken in TAD allows us to investigate questions such as: (1) What are the whole plant consequences of individual traits (Mooney and Chiariello, 1984); (2) How do different traits affect the outcomes of competition (Mooney and Chiariello, 1984); (3) What is the potential for alternative designs of approximately equal performance (Körner, 1991; Farnsworth and Niklas, 1995; Gutschick, 1999); and (4) Which traits are most critical to adaptation in different environments (Mooney and Chiariello, 1984)? We will report the outcome of inquiries on these lines in subsequent papers.

Acknowledgements

We are grateful to the corresponding editor and two anonymous reviewers for their comments. We would like to thank John Sperry for providing Eqs. (36)–(39). David Ackerly, Ken Arii, Jeannine Cavender-Bares, Graham Bell, Marisha Futer, Andrew Gonzalez, Frédéric Guichard, Tapio Linkosalo, Dolph Schluter, and David Tilman have offered constructive critiques during the course of developing this model. We also thank Tarik Gouhier, Frédéric Guichard, and Pradeep Pilai for helpful advice in programming the model. We are grateful to Natural Sciences and Engineering Research Council of Canada, McGill University, and the Groupe de Recherche en Ecologie Forestière interuniversitaire of Montréal for generously providing scholarships to CM. The research was funded by an NSERC grant to MJL.

Appendix A

List of parameters tables with their symbols and units (Tables A1–A3), and supplementary table

Table A1
List of the 34 independent traits in the seedling model

Independent trait variables	Symbol	Range model[a]	Range in nature if known
Fraction storage		0.01–0.11	
Root-to-shoot		0.05–0.35	
Fine-to-thick		0.01–0.41	
Leaf-to-stem		0.2–0.8	
Carbon allocation parameter	a_C	0.1–0.9	
Storage allocation parameter	a_m	0.1–0.9	
Nitrogen allocation parameter	a_N	0.1–0.9	
Carbon allocation parameter	b_C	0.1–0.9	
Storage allocation parameter	b_m	0.1–0.9	
Nitrogen allocation parameter	b_N	0.1–0.9	
Water-use constant	c_1	0.0001–0.01 mol CO_2/mol H_2O	
Water-use exponent	c_2	0.1–10 MPa^{-1}	
Carbon allocation exponent	c_C	0–1	
Storage allocation exponent	c_m	0–7.5	
Nitrogen allocation exponent	c_N	0–1.5	
Mesophyll cell wall thickness	c_w	0.1–6.4 μm	0.3 μm (page 434 in Nobel, 1991)
Leaf cell diameter	d_{cell}	17–80 μm	20–80 μm (Nobel, 1991)
Maximum root depth	d_{max}	15–135 cm	3–78 cm[b]
Fraction of leaf cross-section area that is schlerenchyma	f_{scl}	0–0.07	0–0.06 (Choong et al., 1992)
Maximum stomatal conductance	g_{max}[c]	0.1–2.00 mol CO_2/m^2 s	
Number of mesophyll cell layers in the leaf	Layers	1–16	1–12 (Nobel, 1991)
Maximum leaf area intensity	L_{max}	0.1–3.2 cm^2 leaf/grid cell	
Mesophyll cell nitrogen concentration	N_{cell}	0.005–0.020 g N/g H_2O	0.005–0.020 (Roderick et al., 1999b)
Petiole vs. twig construction cost	Petiole	0.667 for petioles, 1.0 for twigs	
Maximum fine root length intensity	R_{max}	0.1–3.2 cm root/cm^3	
Fine root nitrogen content	R_N	0.02–0.09 gN/g root	0.01–0.03 (our unpublished data)
Stem taper	Taper	0–0.01 cm^2 sapwood/cm stem length	
Cuticle thickness	$t_{cuticle}$	0.5–15.5 × 10^{-4} cm	1.2–15 μm (Choong et al., 1992)
Ratio of xylem wall thickness to vessel radius	w/r	0.05–0.5 for tracheid; 0.01–0.23 for vessels	Hacke et al. (2001)
Maximum crown width	w_{cmax}	15–90 cm to each side	0–177 cm[b]
Maximum root system width	wr_{max}	15–90 cm to each side	0–278 cm[b]
Ratio of stem sapwood area per leaf area	x_{sect1}	0.0001–0.0016 cm^2/cm^2	2.42E−6–0.00335[b] with an avg. 0.000337
Ratio of root sapwood area per fine root length	x_{sect2}	0.00003–0.00048 cm^2/cm	
Depth exponent	δ	$-2 < \delta < +2$	

We refer to traits in TAD as independent if they are independent variables during the optimization of the seedling design. Note to test the realism of the model to produce realistic values the range allowed for each independent trait must be larger than the range found in natural tree seedlings. Therefore, the range of the variables for which published data was available has also been listed in the table.

[a] If units are not given the variable is dimensionless.

[b] Unpublished data for seedlings of 29 southern Quebec tree species. Seedlings in the study were between 2 and 306 cm tall at the time of harvest (at the end of the third growing season).

[c] We measured g_{max} up to 1.8 mol CO_2/m^2 s in seedlings of 28 temperate hardwood tree species (unpublished data). Maximum conductances over 1.0 mol CO_2/m^2 s only occurred in fast-growing shade-intolerant species.

Table A2
List of constants in the model

Constant	Symbol	Units	Value in model
Water holding capacity of the soil grid cell	C	g H_2O/cm^3	Function of the soil type (Brady and Weil, 1999)
Concentration of CO_2 in the air	c_a	ppm	User-specified
Drag coefficient for stem and branch segments	C_{DB}	Dimensionless	1.0 (Table 9.3 in Fox and McDonald, 1992)
Drag coefficient for leaves	C_{DL}	Dimensionless	0.38 (Table 9.3 in Fox and McDonald, 1992)
Nutrient uptake constant	c_{nut}	gN/cm	0.01
Cell wall shade constant	c_{shade1}	μm	4
Chloroplast shade constant	c_{shade2}	μm^{-1}	10
Depth at the middle of the grid cell	d_{depth}	cm	15–135, depending on soil layer
Depth of the lowest soil grid cells	d_{grid}	cm	135
Leaf characteristic length	D_{leaf}	cm	8 (based on effective leaf area)
Diffusion constant for CO_2 at standard conditions	$D^0_{CO_2}$	m^2/s	1.4968E−9 in water 1.33E−5 in air
Fine root diameter	d_{root}	cm	0.05 (Eissenstat, 1992; Fitter, 1996; Pregitzer et al., 2002).
Daily evaporation rate	E_{daily}	g/day cm^2	User-specified
Boundary layer conductance	g_b	mol CO_2/m^2 s	1.0 in model, but 0.2–2.0 in nature (page 399 in Nobel, 1991)
Height at the top of the grid cell	$H_{gridcell}$	cm	30
Light reaction coefficient	k_{light}	μmol/m^{2}s	50
Rate constant	k_{nut}	gN/cm^3	0.000005
Length of branch or stem segment	L	m	0.3 except for stem base which is 0.15
Mesophyll cell photosynthetic sensitivity	m_{photo}	μm/(molCO_2/m^2 s)	15
Maintenance respiration rate per gram of tissue nitrogen	m_{resp}	gC/gN day	1.0368 (estimated from graphed data in Reich et al., 1998b)
Minimum mesophyll cell nitrogen concentration	N_{min}	gN/gH_2O	0.002
Minimum nutrient concentration	$N_{soilmin}$	gN/cm^3	0.000001
Air pressure inside the leaf	P	MPa	101.325
Atmospheric pressure	P^0	MPa	101.325
Resistance to CO_2 diffusion across the mesophyll cell plasmalemma	R_{pl}	s/m	318.31 (Nobel, 1991)
Horizontal area of grid cell	S_{grid}	cm^2	$30 \times 30 = 900$
Effective area of a leaf	s_{leaf}	cm^2	64
Number of days in the simulation	t_{sim}	Days	Set by user (maximum of 1000)
Grid cell volume	$V_{gridcell}$	cm^3	$30 \times 30 \times 30 = 27000$
Width of grid cell	$w_{gridcell}$	cm	30
Nitrogen content of woody tissues	x_N	gN/gC	0.01 (our unpublished data)
Molar fraction gradient of water vapor	$\Delta w = w_i - w_a$	Dimensionless	Used tabulated values as function of temperature
Specific soil conductance	ε	cm/day	Depends on soil type (Brady and Weil, 1999)
Carbon content	ζ	gC/g tissue	0.46 (our unpublished data)
Air viscosity	μ_{air}	kg/(m s)	1.78E−5 (Fox and McDonald, 1992)
Cost of synthesis	ξ	gC/gC	1.35 (Bloom et al., 1985; Chapin, 1989)
Pi	π	Dimensionless	3.1415927
Air density	ρ_{air}	kg/m^3	1.23 (Fox and McDonald, 1992)
Density of leaf cell wall material	$\rho_{cellwall}$	g/cm^3	0.7
Density of xylem wall material	ρ_x	g/cm^3	1 (Hacke et al., 2001)
Cell wall shear stress	τ	MPa	3
Head to MPa	χ	cm/MPa	10204

A reference is given for values of constants taken from the literature. Explanations for estimates of constants not from the literature are found in the respective sections of the model description.

Table A3
List of symbols for dependent variables in the model

Parameter	Symbol	Units
Photosynthetic rate	A	gC/cm^2 day
Branch or stem cross-section area	A_b	m^2
Seedling's total vertical branch cross section area in the grid cell	A_{branch}	m^2
Seedling's total leaf area in the grid cell	A_{leaf}	m^2
Allocation of carbon to above vs. below ground growth	$Allo_C$	Dimensionless fraction
Allocation to storage for maintenance	$Allo_m$	Dimensionless fraction
Allocation of carbon to above vs. below ground growth	$Allo_N$	Dimensionless fraction
Horizontal area occupied by a mesophyll cell	A_{mes}	μm^2
Total carbon in the leaves of the seedling	B_L	gC
Total carbon in fine roots of the seedling	B_R	gC
Total carbon in stems and branches of the seedling	B_S	gC
Total dry mass of the seedling	B_{total}	g dry mass
Total carbon in thick roots of the seedling	B_{TR}	gC
CO_2 concentration inside mesophyll cells in layer n	$c_{c,n}$	Dimensionless
CO_2 concentration inside the substomatal cavity	c_i	Dimensionless
Soil conductance	C_s	g H_2O/MPa day
Soil distance	D	cm
Diffusion constant for CO_2	$D^0_{CO_2}$	m^2/s
Transpiration rate	E	g H_2O/cm^2 day
Modulus of elasticity	E_{MOE}	Pa
Total transpiration from grid cell n	E_n	g H_2O/day
Soil evaporation	E_{vap}	g H_2O
Drag force	F_D	N
Mechanical factor of safety	FS	Dimensionless
Combined internal leaf conductance	g_i	mol CO_2/(m^2 s)
Cuticular conductance	g_{min}	mol H_2O/m^2 s
Stomatal conductance	g_s	mol CO_2/m^2 s
Light intensity in the canopy	I	μmol/m^2 s
Light intensity above the canopy	I_0	μmol/m^2 s
Light intensity incident on the leaf surface	I_{in}	μmol/m^2 s
Relative light level	I_{level}	Dimensionless fraction
Modulus of inertia	I_{MOI}	m^4
Sap-flow in root n	i_n	g H_2O/day
Conductance	K	g H_2O/MPa day
Path length of branch	L_b	cm
Leaf area intensity threshold	L_{int}	cm^2/cm^2 grid cell
Leaf longevity	L_{long}	Weeks
Leaf nitrogen content	L_N	gN/gC
Path length of root	L_r	cm
Mechanical moment	M	Nm
Total maintenance respiration rate	M_{RESP}	gC/day
Number of leaves in grid cell	N	Dimensionless
Nutrient concentration in the soil solution	N_{soil}	gN/cm^3
Osmotic potential	osm	MPa
Mechanical force	P	N
Photosynthetic rate of a mesophyll cell in layer n	P_n	gC/day
Radius of stem or branch segment or tap root at the base	R	m
Resistance to CO_2 diffusion across mesophyll cell walls	R_{cw}	s/m
Resistance to CO_2 diffusion in the mesophyll cell cytosol	R_{cy}	s/m
Reynolds number	Re	Dimensionless
Resistance to CO_2 diffusion in the leaf internal air space	R_{ias}	s/m
Fine root length intensity threshold	R_{int}	cm/grid cell
Root length	R_L	cm

Table A3 (*Continued*)

Parameter	Symbol	Units
Hydraulic resistance of branch going to grid cell *n*	R_{Ln}	(MPa day)/g H_2O
Fine root longevity	R_{long}	Weeks
Hydraulic resistance of root *n*	R_{Rn}	(MPa day)/g H_2O
Hydraulic resistance of soil grid cell *n*	R_{Sn}	(MPa day)/g H_2O
Leaf internal shading constant due to chloroplasts	sc_{chl}	Dimensionless
Leaf internal shading constant due to cell walls	sc_{w}	Dimensionless
Root surface area	s_{root}	cm^2
Absolute temperature of the leaf	T	K
Time	Time	Timestep/year
Turgor of leaves in grid cell *n*	T_{Ln}	MPa
Volume of leaf cell wall	$V_{cellwall}$	cm^3
Volume of leaf cuticle	$V_{cuticle}$	cm^3
Light reaction coefficient 1	ν_{light}	mol CO_2/m^2 s
Mesophyll cell volume	V_{mes}	μm^3
Volume of leaf schlerenchyma	V_{schl}	cm^3
Wind speed	V_{wind}	m/s
Volume of wood	V_{wood}	cm^3
Deflection due to mechanical loading	Y	m
Leaf cell layer	Z	Dimensionless
Construction cost	α	gC
Xylem cross-section area	β	cm^2
Water content of the soil grid cell	θ	g H_2O/cm^3
Xylem conductivity	κ_{xy}	g H_2O/cm MPa day
Water-use level	ν_{water}	mol CO_2/mol H_2O
Failure stress under compression	Σ_{comp}	Pa
Maximum stress	Σ_{max}	Pa
Rate of active nutrient uptake	Φ	gN/cm^2 surface area
Maximum rate of active nutrient uptake	φ_{max}	gN/cm
Leaf water potential	Ψ_L	MPa
Root water potential	Ψ_R	MPa
Soil water potential	Ψ_s	MPa
Xylem water potential	Ψ_x	MPa
Minimum xylem water potential	$\Psi_{x,min}$	MPa

We refer to traits in TAD as independent if they are independent variables during the optimization of the seedling design. Other variables that are calculated from these independent variables are referred to as dependent variables.

Table A4
List of values for ecophysiological traits in the model tree seedling compared to their range in natural tree seedlings

Dependent trait	Range in model tree seedling	Range in natural trees	References
Maximum photosynthetic rate (μmol/m^2s)	18	3–24	Reich et al. (1999), Prior et al. (2003); our unpublished data
Leaf longevity (weeks)	52	6–450	Reich et al. (1999)
Leaf blade nitrogen concentration (i.e. petioles not included) (%)	4.9	0.6–4.3	Reich et al. (1999), Prior et al. (2003); our unpublished data
Leaf mass per area (g/m^2)	48	14–833	Reich et al. (1998b), Reich et al. (1999)
Leaf thickness (μm)	331	65–1296	Cavelier (1990), Choong et al. (1992), Holbrook and Putz (1996), Niinemets (2001), Prior et al. (2003)

Table A4 (*Continued*)

Dependent trait	Range in model tree seedling	Range in natural trees	References
Minimum cuticular conductance (mol H_2O/cm^2 s)	150	4–160	Nobel (1991)
Productivity water-use-efficiency (g dry mass/kg H_2O)	0.7	1–6	Larcher (2003)
Average daily water-use-efficiency (gC/kg H_2O)	2.4	0.9–6	Ehleringer et al. (1985)
Maximum sap-flow rate per leaf area (g/m^2h)	545	21–1611	Our unpublished data[a]
Maximum sap-flow rate per stem basal area (g/cm^2h)	310	14–1330	Our unpublished data[a]
Huber value (cm^2 wood/m^2 leaf area)	2.4	0.1–33.5	Our unpublished data[a]
Leaf water potential at wilting point (MPa)	1.2	0.8–7	Cavelier (1990), Holbrook and Putz (1996), Niinemets (2001), Groom (2004)
Minimum xylem water potential (MPa)	2.9	1–12	Hacke et al. (2001)
Wood density (g/cm^3)	0.56	0.16–1.05	Forest Products Laboratory (1999)
Specific root length (m/g)	9	20–300	Reich et al. (1998b), Espeleta and Donovan (2002), Comas et al. (2002)
% Nitrogen uptake that was passive	69	0.5 in tundra, 80 in corn field	Lambers et al. (1998)
Height-to-basal diameter ratio	147	8–164	Our unpublished data[a]
Root area index (cm^2 fine root surface area/cm^2 ground)	1.4	0.05–10[b]	Larcher (2003)
Leaf area index (cm^2 leaf area/cm^2 ground)	3.7	3–16[c]	Larcher (2003)

Traits were chosen because ecophysiologists commonly measure them and published data was readily available (references given in the right column).

[a] Our unpublished data is for seedlings of 29 tree species native to southern Quebec.

[b] For seedlings 0.05–2.4, up to 10 for dense conifer stands, less for deciduous trees, and 2–4 for shrubs.

[c] For adult trees whose LAI should be higher than for seedlings. Highest LAI's are for conifers.

with descriptive results of the model tree seedling (Table A4).

References

Aerts, R., Chapin, F.S., 2000. The mineral nutrition of wild plants revisited: a re-evaluation of processes and patterns. Adv. Ecol. Res. 30, 1–67.

Bargel, H., Barthlott, W., Koch, K., Schreiber, L., Neinhaus, C., 2004. Plant cuticles: mulitfunctional interfaces between plant and environment. In: Hemsley, A.R., Poole, I. (Eds.), The Evolution of Plant Physiology from Whole Plants to Ecosystems. Elsevier Academic Press, London, UK, pp. 171–197.

Bateman, R.M., Crane, P.R., DiMichele, W.A., Kenrick, P.R., Rowe, N.P., Speck, T., Stein, W.E., 1998. Early evolution of land plants: phylogeny, physiology, and ecology of the primary terrestrial radiation. Annu. Rev. Ecol. Syst. 29, 263–292.

Beer, F.P., Johnston, E.R., 1985. Mechanics of Materials. McGraw-Hill Ryerson Ltd., Toronto, Ont., Canada.

Biswell, H.H., 1935. Effects of environment upon the root habits of certain deciduous forest trees. Bot. Gazette 96, 676–708.

Bloom, A.J., Chapin, F.S., Mooney, H.A., 1985. Resource limitation in plants—an economic analogy. Annu. Rev. Ecol. Syst. 16, 363–392.

Borchert, R., 1994. Soil and stem water storage determine phenology and distribution of tropical dry forest trees. Ecology 75, 1437–1449.

Bossomaier, T.R.J., Green, D.G., 2000. Complex Systems. Cambridge University Press, Cambridge, UK.

Brady, N.C., Weil, R.R., 1999. The Nature and Properties of Soils. Prentice Hall, Upper Saddle River, NJ, USA.

Bressan, R.A., 1998. Stress physiology. In: Taiz, L., Zeiger, E. (Eds.), Plant Physiology. Sinauer Associates Inc., Sunderland, MA, USA, pp. 726–730.

Brodribb, T.J., Holbrook, N.M., Edwards, E.J., Gutiérrez, M.V., 2003. Relations between stomatal closure, leaf turgor and xylem vulnerability in eight tropical dry forest trees. Plant Cell Environ. 26, 443–450.

Buckley, T.N., Miller, J.M., Farquhar, G.D., 2002. The mathematics of linked optimization for water and nitrogen use in a canopy. Silva Fennica 36, 639–669.

Burgess, S.S.O., Adams, M.A., Turner, N.C., Ong, C.K., 1998. The redistribution of soil water by tree root systems. Oecologia 115, 306–311.

Burgess, S.S.O., Adams, M.A., Turner, N.C., White, D.A., Ong, C.K., 2001. Tree roots: conduits for deep recharge of soil water. Oecologia 126, 158–165.

Caldwell, M.M., Richards, J.H., 1989. Hydraulic lift: water efflux from upper roots improves effectiveness of water uptake by deep roots. Oecologia 79, 1–5.

Cavelier, J., 1990. Tissue water relations in elfin cloud forest tree species of Serrania de Macuira, Guajira, Colombia. Trees 4, 155–163.

Chapin, F.S., 1989. The cost of tundra plant structures: evaluation of concepts and currencies. Am. Nat. 133, 1–19.

Chen, J.-L., Reynolds, J.F., 1997. A coordination model of whole-plant carbon allocation in relation to water stress. Ann. Bot. 80, 45–55.

Choong, M.F., Lucas, P.W., Ong, J.S.Y., Pereira, B., Tan, H.T.W., Turner, I.M., 1992. Leaf fracture toughness and sclerophylly: their correlations and ecological implications. New Phytol. 121, 597–610.

Cochard, H., Coll, L., Le Roux, X., Améglio, T., 2002. Unraveling the effects of plant hydraulics on stomatal closure during water stress in walnut. Plant Physiol. 128, 282–290.

Cohen, D., 1970. The expected efficiency of water utilization in plants under different competition and selection regimes. Israel J. Bot. 19, 50–54.

Coleman, J.S., McConnaughay, K.D.M., Ackerly, D.D., 1994. Interpreting phenotypic variation in plants. Trends Ecol. Evolut. 9, 187–191.

Comas, L.H., Bouma, T.J., Eissenstat, D.M., 2002. Linking root traits to potential growth rate in six temperate tree species. Oecologia 132, 34–43.

Comas, L.H., Eissenstat, D.M., 2004. Linking fine root traits to maximum potential growth rate among 11 mature temperate tree species. Funct. Ecol. 18, 388–397.

Coutts, M.P., 1983. Root architecture and tree stability. Plant Soil 71, 171–188.

Cowan, I.R., 1982. Regulation of water use in relation to carbon gain in higher plants. In: Lange, O.L., Nobel, P.S., Osmond, C.B., Ziegler, H. (Eds.), Physiological Plant Ecology II: Water Relations and Carbon Assimilation. Springer, Berlin, Germany, pp. 589–612.

Cowan, I.R., Farquhar, G.D., 1977. Stomatal function in relation to leaf metabolism and environment. In: Jennings, D.H. (Ed.), Integration of Activity in Higher Plants. Cambridge University Press, Cambridge, UK, pp. 471–505.

Crocker, J.L., Witte, W.T., Augé, R.M., 1998. Stomatal sensitivity of six temperate, deciduous tree species to non-hydraulic root-to-shoot signaling of partial soil drying. J. Exp. Bot. 49, 761–774.

Cui, M., Vogelmann, T.C., Smith, W.K., 1991. Chlorophyll and light gradients in sun and shade leaves of *Spinacia oleracea*. Plant Cell Environ. 14, 493–500.

Dawson, T.E., 1993. Hydraulic lift and water use by plants: implications for water balance, performance and plant–plant interactions. Oecologia 95, 565–574.

Díaz, S., Hodgson, J.G., Thompson, K., Cabido, M., Cornelissen, J.H.C., Jalili, A., Montserrat-Martí, G., Grime, J.P., Zarrinkamar, F., Asri, Y., Band, S.R., Basconselo, S., Castro-Díez, P., Funes, G., Hamzehee, B., Khoshnevi, M., Pérez-Rontomé, M.C., Shirvany, F.A., Vendramini, F., Yazdani, S., Abbas-Azimi, R., Bogaard, A., Boustani, S., Charles, M., Dehghan, M., de Torres-Espuny, L., Falczuk, V., Guerrero-Campo, J., Hynd, A., Jones, G., Kowsary, E., Kazemi-Saeed, F., Maestro-Martínez, M., Romo-Díez, A., Shaw, S., Siavash, B., Villar-Salvador, P., Zak, M.R., 2004. The plant traits that drive ecosystems: Evidence from three continents. J. Veg. Sci. 15, 295–304.

Donovan, L.A., Linton, M.J., Richards, J.H., 2001. Predawn plant water potential does not necessarily equilibrate with soil water potential under well-watered conditions. Oecologia 129, 328–335.

Eamus, D., Prichard, H., 1998. A cost-benefit analysis of leaves of four Australian savanna species. Tree Physiol. 18, 537–545.

Ehleringer, J.R., Schulze, E.-D., Ziegler, H., Lange, O.L., Farquhar, G.D., Cowan, I.R., 1985. Xylem-tapping mistletoes: water or nutrient parasites? Science 227, 1479–1481.

Eissenstat, D.M., 1991. On the relationship between specific root length and the rate of root proliferation: a field study using citrus rootstocks. New Phytol. 118, 63–68.

Eissenstat, D.M., Wells, C.E., Yanai, R.D., Whitbeck, J.L., 2000. Building roots in a changing environment: implications for root longevity. New Phytol. 147, 33–42.

Eissenstat, D.M., Yanai, R.D., 1997. The ecology of root lifespan. Adv. Ecol. Res. 27, 1–60.

Eissenstat, D.M., 1992. Costs and benefits of constructing roots of small diameter. J. Plant Nutrit. 15, 763–782.

Ellis, G.F.R., 2005. Physics, complexity and causality. Nature 435, 743.

Ennos, A.R., 1993. The scaling of root anchorage. J. Theor. Biol. 161, 61–75.

Ennos, A.R., 1994. The biomechanics of root anchorage. Biomimetics 2, 129–137.

Ennos, A.R., 2000. The mechanics of root anchorage. Adv. Bot. Res. 33, 133–157.

Ennos, A.R., Fitter, A.H., 1992. Comparative functional morphology of the anchorage systems of annual dicots. Funct. Ecol. 6, 71–78.

Espeleta, J.F., Donovan, L.A., 2002. Fine root demography and morphology in response to soil resources availability among xeric and mesic sandhill tree species. Funct. Ecol. 16, 113–121.

Evans, C.G., 1972. The Quantitative Analysis of Plant Growth. University of California Press, Berkeley, CA, USA.

Farnsworth, K.D., Niklas, K.J., 1995. Theories of optimization, form and function in branching architecture in plants. Funct. Ecol. 9, 355–363.

Farquhar, G.D., Buckley, T.N., Miller, J.M., 2002. Optimal stomatal control in relation to leaf area and nitrogen content. Silva Fennica 36, 625–637.

Fitter, A., 1996. Characteristics and functions of root systems. In: Waisel, Y., Eshel, A., Kafkafi, U. (Eds.), Plant Roots: The Hidden Half. Marcel Dekker Inc., New York, NY, USA, pp. 1–20.

Forest Products Laboratory, 1999. Wood Handbook, Wood as an Engineering Material, General Technical Report FPL-GTR-113. USDA Forest Service, USA.

Fox, R.W., McDonald, A.T., 1992. Introduction to Fluid Mechanics. John Wiley & Sons Inc., New York, NY, USA.

Gartner, B.L., 1995. Patterns of xylem variation within a tree and their hydraulic and mechanical consequences. In: Gartner, B.L. (Ed.), Plant Stems: Physiology and Functional Morphology. Academic Press, San Diego, CA, USA, pp. 125–149.

Geber, M.A., Griffen, L.R., 2003. Inheritance and natural selection on functional traits. Int. J. Plant Sci. 164, S21–S42.

Genard, M., Pages, L., Kervella, J., 1998. A carbon balance model of peach tree growth and development for studying the pruning response. Tree Physiol. 18, 351–362.

Gill, R.A., Jackson, R.B., 2000. Global patterns of root turnover for terrestrial ecosystems. New Phytol. 147, 13–31.

Givnish, T.J., 1986a. On the Economy of Plant form and Function. Cambridge University Press, Cambridge, UK.

Givnish, T.J., 1986b. Optimal stomatal conductance, allocation of energy between leaves and roots, and the marginal cost of transpiration. In: Givnish, T.J. (Ed.), On the Economy of Plant Form and Function. Cambridge University Press, Cambridge, UK, pp. 171–213.

Givnish, T.J., 1995. Plant Stems: biomechanical adaptation for energy capture and influence on species distributions. In: Gartner, B.L. (Ed.), Plant Stems: Physiology and Functional Morphology. Academic Press, San Diego, CA, USA, pp. 3–49.

Goldberg, D.E., 1989. Genetic Algorithms in Search, Optimization, and Machine Learning. Addison-Wesley Publishing Company Inc., Reading, MA, USA.

Greenhill, A.G., 1881. Determination of the greatest height consistent with the stability that a vertical pole or mast can be made, and of the greatest height to which a tree of given proportions can grow. Proc. Cambridge Philos. Soc. 4, 65–73.

Groom, P.K., 2004. Rooting depth and plant water relations explain species distribution patterns within a sandplain landscape. Funct. Plant Biol. 31, 423–428.

Guthrie, R.L., 1989. Xylem structure and ecological dominance in a forest community. Am. J. Bot. 76, 1216–1228.

Gutschick, V.P., 1999. Biotic and abiotic consequences of differences in leaf structure. New Phytol. 143, 3–18.

Hacke, U.G., Sperry, J.S., 2001. Functional and ecological xylem anatomy. Perspect. Plant Ecol. Evol. Syst. 4, 97–115.

Hacke, U.G., Sperry, J.S., Pockman, W.T., Davis, S.D., McCulloh, K.A., 2001. Trends in wood density and structure are linked to prevention of xylem implosion by negative pressure. Oecologia 126, 457–461.

Harcombe, P.A., 1987. Tree life tables. Simple birth, growth, and death data encapsulate life histories and ecological role. BioScience 37, 557–568.

Hari, P., Mäkelä, A., Korpilahti, E., Holmberg, M., 1986. Optimal control of gas exchange. Tree Physiol. 2, 169–175.

Hikosaka, K., Hirose, T., 1998. Leaf and canopy photosynthesis of C_3 plants at elevated CO_2 in relation to optimal partitioning of nitrogen among photosynthetic components: theoretical prediction. Ecol. Model. 106, 247–259.

Hilbert, D.W., 1990. Optimization of plant root:shoot ratios and internal nitrogen concentration. Ann. Bot. 66, 91–99.

Hilbert, D.W., Larigauderie, A., Reynolds, J.F., 1991. The influence of carbon dioxide and daily photon-flux density on optimal leaf nitrogen concentration and root:shoot ratio. Ann. Bot. 68, 365–376.

Hoch, G., Richter, A., Körner, Ch., 2003. Non-structural carbon compounds in temperate forest trees. Plant Cell Environ. 26, 1067–1081.

Holbrook, N.M., Putz, F.E., 1996. From epiphyte to tree: differences in leaf structure and leaf water relations associated with the transition in growth form in eight species off hemiepiphytes. Plant Cell Environ. 19, 631–642.

Holch, A.E., 1931. Development of roots and shoots of certain deciduous tree seedlings in different forest sites. Ecology 12, 259–298.

Iwasa, Y., Cohen, D., Leon, J.A., 1984. Tree height and crown shape, as results of competitive games. J. Theor. Biol. 112, 279–297.

Jackson, R.B., Lechowicz, M.J., Li, X., Mooney, H.A., 2001. The roles of phenology, growth and allocation in global terrestrial productivity. In: Mooney, H.A., Roy, J. (Eds.), Terrestrial Global Productivity: Past, Present and Future. Academic Press, New York, NY, USA, pp. 61–82.

Kerstiens, G., 1996. Cuticular water permeability and its physiological significance. J. Exp. Bot. 47, 1813–1832.

Khalil, A.A.M., Grace, J., 1993. Does xylem sap ABA control the stomatal behavior of water-stressed sycamore (*Acer pseudoplatanus* L.) seedlings? J. Exp. Bot. 44, 1127–1134.

King, D.A., 1981. Tree dimensions: maximizing the rate of height growth in dense stands. Oecologia 51, 351–356.

King, D.A., 1986. Tree form, height growth, and susceptibility to wind damage in *Acer saccharum*. Ecology 67, 980–990.

King, D.A., 1990. The adaptive significance of tree height. Am. Nat. 135, 809–827.

King, D.A., 1993. A model analysis of the influence of root and foliage allocation on forest production and competition between trees. Tree Physiol. 12, 119–135.

King, D.A., Loucks, O.L., 1978. The theory of tree bole and branch form. Radiat. Environ. Biophys. 15, 141–165.

Körner, C., 1991. Some often overlooked plant characteristics as determinants of plant growth: a reconsideration. Funct. Ecol. 5, 162–173.

Körner, C., 2003. Carbon limitation in trees. J. Ecol. 91, 4–17.

Kozlowski, T.T., Pallardy, S.G., 1997. Physiology of Woody Plants. San Diego, Academic Press.

Kramer, P.J., Boyer, J.S., 1995. Water relations of Plants and Soils. Academic Press, San Diego, CA, USA.

Laland, K.N., Ddling-Smee, J., Feldman, M.W., 2004. Causing a commotion. Nature 429, 609.

Lambers, H., Chapin, F.S., Pons, T.L., 1998. Plant Physiological Ecology. Springer, New York, NY, USA.

Lambers, H., Poorter, H., 2004. Inherent variation in growth rate between higher plants: a search for physiological causes and ecological consequences. Adv. Ecol. Res. 34, 283–362.

Landis, M.R., Peart, D.R., 2005. Early performance predicts canopy attainment across life histories in subalpine forest trees. Ecology 86, 63–72.

Larcher, W., 2003. Physiological Plant Ecology. Springer, Berlin, Germany.

Ledig, F.T., Drew, A.P., Clark, J.G., 1976. Maintenance and constructive respiration, photosynthesis, and net assimilation rate in seedlings of pitch pine (*Pinus rigida* Mill.). Ann. Bot. 40, 289–300.

Loescher, W.H., McCamant, T., Keller, J.D., 1990. Carbohydrate reserves, translocation, and storage in woody plant roots. HortScience 25, 274–279.

Loewenstein, N.J., Pallardy, S.G., 1998. Drought tolerance, xylem sap abscisic acid and stomatal conducance during soil drying: a comparison of young plants of four temperate deciduous angiosperms. Tree Physiol. 18, 421–430.

Lucas, P.W., Turner, I.M., Dominy, N.J., Yamashita, N., 2000. Mechanical defenses to herbivory. Ann. Bot. 86, 913–920.

Magnani, F., Grace, J., Borghetti, M., 2002. Adjustment of tree structure in response to the environment under hydraulic constraints. Funct. Ecol. 16, 385–393.

Maherali, H., Pockman, W.T., Jackson, R.B., 2004. Adaptive variation in the vulnerability of woody plants to xylem cavitation. Ecology 85, 2184–2199.

Mäkelä, A., Berninger, F., Hari, P., 1996. Optimal control of gas exchange during drought: theoretical analysis. Ann. Bot. 77, 461–467.

Mäkelä, A., Givnish, T.J., Berninger, F., Buckley, T.N., Farquhar, G.D., Hari, P., 2002. Challenges and opportunities of the optimality approach in plant ecology. Silva Fennica 36, 605–614.

Mattheck, C., Bethge, K., Albrecht, W., 1995. Failure modes of trees and related failure criteria. In: Coutts, M.P., Grace, J. (Eds.), Wind and Trees. Cambridge University Press, Cambridge, UK, pp. 195–203.

Mattheck, C., 1998. Design in Nature: Learning from Trees. Springer-Verlag, Berlin.

Maynard Smith, J., 1982. Evolution and the Theory of Games. Cambridge University Press, Cambridge, UK.

Meinzer, F.C., 2003. Functional convergence in plant responses to the environment. Oecologia 134, 1–11.

Mencuccini, M., 2002. Hydraulic constraints in the functional scaling of trees. Tree Physiol. 22, 553–565.

Mitchell, M., 1996. An Introduction to Genetic Algorithms. The MIT Press, Cambridge, MA, USA.

Monsi, M., Saeki, T., 1953. Über den Lichtfaktor in den Pflanzengesellschaften und seine Bedeutung für die Stoffproduktion. Jap. J. Bot. 14, 22–52.

Mooney, H.A., Gulmon, S.L., 1979. Environmental and evolutionary constraints on the photosynthetic characteristics of higher plants. In: Solbrig, O.T., Jain, S., Johnson, G.B., Raven, P.H. (Eds.), Topics in Plant Population Biology. Columbia University Press, New York, NY, USA, pp. 316–337.

Mooney, H.A., Chiariello, N.R., 1984. The study of plant function—the plant as a balanced system. In: Dirzo, R., Sarukhán, J. (Eds.), Perspectives on Plant Population Ecology. Sinauer Associates Inc., Sunderland, MA, USA, pp. 305–323.

Neild, S.A., Wood, C.J., 1999. Estimating stem and root-anchorage flexibility in trees. Tree Physiol. 19, 141–151.

Niinemets, Ü., 2001. Global-scale climatic controls of leaf dry mass per area, density, and thickness in trees and shrubs. Ecology 82, 453–469.

Niinemets, Ü., Portsmuth, A., Truus, L., 2002. Leaf structural and photosynthetic characteristics, and biomass allocation to foliage in relation to foliar nitrogen content and tree size in three *Betula* species. Ann. Bot. 89, 191–204.

Nikinmaa, E., 1992. The allocation of carbohydrates. In: Salminen, H., Katerman, T. (Eds.), Simulation of Forrest Development. Finnish Forest Research Institute, pp. 21–34.

Niklas, K.J., 1994a. The allometry of safety-factor for plant height. Am. J. Bot. 81, 345–351.

Niklas, K.J., 1994b. Interspecific allometries of critical buckling height and actual plant height. Am. J. Bot. 81, 1275–1279.

Niklas, K.J., 1994c. Morphological evolution through complex domains of fitness. Proc. Natl. Acad. Sci. U.S.A. 91, 6772–6779.

Niklas, K.J., 1998. The influence of gravity and wind on land plant evolution. Rev. Paleobot. Palynol. 102, 1–14.

Niklas, K.J., 1999. Changes in the factor of safety within the superstructure of a dicot tree. Am. J. Bot. 86, 688–696.

Niklas, K.J., 2000. Computing factors of safety against wind-induced tree stem damage. J. Exp. Bot. 51, 797–806.

Niklas, K.J., 2004. Computer models of early land plant evolution. Annu. Rev. Earth Planet. Sci. 32, 47–66.

Nobel, P.S., 1977. Internal leaf area and cellular CO_2 resistance: photosynthetic implications of variations with growth conditions and plant species. Physiol. Plant. 40, 137–144.

Nobel, P.S., 1980. Leaf anatomy and water use efficiency. In: Turner, N.C., Kramer, P.J. (Eds.), Adaptation of Plants to Water and high Temperature Stress. Wiley Interscience, New York, NY, USA, pp. 43–55.

Nobel, P.S., 1991. Physicochemical and Environmental Plant Physiology. Academic Press, San Diego, CA.

Oliver, C.D., Larson, B.C., 1996. Forest Stand Dynamics. John Wiley & Sons Inc., New York, NY, USA.

Orians, G.H., Solbrig, O.T., 1977. A cost-income model of leaves and roots with special reference to arid and semiarid areas. Am. Nat. 111, 677–690.

Parker, G.A., Maynard Smith, J., 1990. Optimality theory in evolutionary biology. Nature 348, 27–33.

Patton, L., Jones, M.B., 1989. Some relationships between leaf anatomy and photosynthetic characteristics of willows. New Phytol. 111, 657–661.

Pearcy, R.W., 1989. Plant Physiological Ecology: Field Methods and Instrumentation. Chapman and Hall, London, UK.

Perttunen, J., Sievanen, R., Nikinmaa, E., Salminen, H., Saarenmaa, H., Vakeva, J., 1996. LIGNUM: a tree model based on simple structural units. Ann. Bot. 77, 87–98.

Pigliucci, M., 2004. Studying the plasticity of phenotypic integration in a model organism. In: Pigliucci, M., Preston, K. (Eds.), Phenotypic Integration: Studying the Ecology and Evolution of Complex Phenotypes. Oxford University Press, Oxford, UK, pp. 155–175.

Pigliucci, M., 2005. Evolution of phenotypic plasticity: where are we going now? Trends Ecol. Evol. 20, 481–486.

Pregitzer, K.S., DeForest, J.L., Burton, A.J., Allen, M.F., Ruess, R.W., Hendrick, R.L., 2002. Fine root architecture of nine North American trees. Ecol. Monogr. 72, 293–309.

Preston, K.A., Ackerly, D.D., 2004. The evolution of allometry in modular organisms. In: Pigliucci, M., Preston, K. (Eds.), Phenotypic Integration: Studying the ecology and evolution of complex phenotypes. Oxford University Press, Oxford, UK, pp. 80–106.

Prior, L.D., Eamus, D., Bowman, D.M.J.S., 2003. Leaf attributes in the seasonally dry tropics: a comparison of four habitats in northern Australia. Funct. Ecol. 17, 504–515.

Proulx, S.R., Promislow, D.E.L., Phillips, P.C., 2005. Network thinking in ecology and evolution. Trends Ecol. Evol. 20, 345–353.

Reich, P.B., Wright, I.J., Cavender-Bares, J., Craine, J.M., Oleksyn, J., Westoby, M., Walters, M.B., 2003. The evolution of plant functional variation: traits, spectra, and strategies. Int. J. Plant Sci. 164, S143–S164.

Reich, P.B., Ellsworth, D.S., Walters, M.B., Vose, J.M., Gresham, C., Volin, J.C., Bowman, W.D., 1999. Generality of leaf trait relationships: a test across six biomes. Ecology 80, 1955–1969.

Reich, P.B., Walters, M.B., Tjoelker, D., Vanderklein, D., Buschena, C., 1998a. Photosynthesis and respiration rates depend on leaf and root morphology and nitrogen concentration in nine boreal

tree species differing in relative growth rate. Funct. Ecol. 12, 395–405.

Reich, P.B., Walters, M.G., Tjoelker, D., Vanderklein, D., Buschena, C., 1998b. Photosynthesis and respiration rates depend on leaf and root morphology and nitrogen concentration in nine boreal tree species differing in relative growth rate. Funct. Ecol. 12, 395–405.

Reich, P.B., Walters, M.B., Ellsworth, D.S., 1997. From tropics to tundra: global convergence in plant functioning. Proc. Natl. Acad. Sci. U.S.A. 94, 13730–13734.

Roderick, M.L., Berry, S.L., Noble, I.R., 2000. A framework for understanding the relationship between environment and vegetation based on the surface area to volume ratio of leaves. Funct. Ecol. 14, 423–437.

Roderick, M.L., Berry, S.L., Noble, I.R., Farquhar, G.D., 1999a. A theoretical approach to linking the composition and morphology with the function of leaves. Funct. Ecol. 13, 683–695.

Roderick, M.L., Berry, S.L., Saunders, A.R., Noble, I.R., 1999b. On the relationship between the composition, morphology and function of leaves. Funct. Ecol. 13, 696–710.

Rowe, N., Speck, T., 2004. Hydraulics and mechanics of plants: novelty, innovation and evolution. In: Hemsley, A.R., Poole, I. (Eds.), The Evolution of Plant Physiology from Whole Plants to Ecosystems. Elsevier Academic Press, London, UK, pp. 297–325.

Sack, L., Cowan, P.D., Jaikumar, N., Holbrook, N.M., 2003. The 'hydrology' of leaves: co-ordination of structure and function in temperate woody species. Plant Cell Environ. 26, 1343–1356.

Schieving, F., Poorter, H., 1999. Carbon gain in a multispecies canopy: the role of specific leaf area and photosynthetic nitrogen-use efficiency in the tragedy of the commons. New Phytol. 143, 201–211.

Schulze, E.-D., Caldwell, M.M., Canadell, J., Mooney, H.A., Jackson, R.B., Parson, D., Scholes, R., Sala, O.E., Trimborn, P., 1998. Downward flux of water through roots (i.e. inverse hydraulic lift) in dry Kalahari sands. Oecologia 115, 460–462.

Schulze, E.-D., Schilling, K., Nagarajah, S., 1983. Carbohydrate partitioning in relation to whole plant production and water use of *Vigna unguiculata* (L.) Walp. Oecologia 58, 169–177.

Schwinning, S., Ehleringer, J.R., 2001. Water use tradeoffs and optimal adaptations to pulse-driven arid ecosystems. J. Ecol. 89, 464–480.

Shipley, B., Lechowicz, M.J., 2000. The functional co-ordination of leaf morphology, nitrogen concentration, and gas exchange in 40 wetland species. Ecoscience 7, 183–194.

Shugart, H.H., 1997. Plant and ecosystem functional types. In: Smith, T.M., Shugart, H.H., Woodward, F.I. (Eds.), Plant Functional Types: Their Relevance to Ecosystem Properties and Global Change. Cambridge University Press, Cambridge, UK, pp. 20–44.

Sperry, J.S., 1995. Limitations on stem water transport and their consequences. In: Gartner, B.L. (Ed.), Plant Stems: Physiology and Functional Morphology. Academic Press, San Diego, CA, USA.

Sperry, J.S., 2003. Evolution of water transport and xylem structure. Int. J. Plant Sci. 164, S115–S127.

Stout, B.B., 1956. Studies of the root systems of deciduous trees. Black Rock For. Bull. 15, 3–45.

Stuefer, J.F., During, H.J., Schieving, F., 1998. A model on optimal root-shoot allocation and water transport in clonal plants. Ecol. Model. 111, 171–186.

Suding, K.N., Collins, S.L., Gough, L., Clark, C., Cleland, E.E., Gross, K.L., Milchunas, D.G., Pennings, S., 2005. Functional- and abundance-based mechanisms explain diversity loss due to N fertilization. Proc. Natl. Acad. Sci. U.S.A. 102, 4387–4392.

Sultan, S.E., Bazzaz, F.A., 1993a. Phenotypic plasticity in *Polygonum persicaria*: I. Diversity and uniformity of genotypic norms of reaction to light. Evolution 47, 1009–1031.

Sultan, S.E., Bazzaz, F.A., 1993b. Phenotypic plasticity in *Polygonum persicaria*. II. Norms of reaction to soil moisture and the maintenance of genetic diversity. Evolution 47, 1032–1049.

Sultan, S.E., Bazzaz, F.A., 1993c. Phenotypic plasticity in *Polygonum persicaria*. III. The evolution of ecological breadth for nutrient environment. Evolution 47, 1050–1071.

Sutherland, W.J., 2005. The best solution. Nature 435, 569.

Tenhunen, J.D., Hanano, R., Abril, M., Weiler, E.W., Hartung, W., 1994. Above- and below-ground environmental influences on leaf conductance of *Ceanothus thyrsiflorus* growing in a chaparral environment: drought response and the role of abscisic acid. Oecologia 99, 306–314.

Tenhunen, J.D., Pearcy, R.W., Lange, O.L., 1987. Diurnal variations in leaf conductance and gas exchange in natural environments. In: Zeiger, E., Farquhar, G.D., Cowan, I.R. (Eds.), Stomatal Function. Stanford University Press, Stanford, CA, USA, pp. 323–351.

Thomas, F.M., 2000. Vertical rooting patterns of mature *Quercus* trees growing on different soil types in northern Germany. Plant Ecol. 147, 95–103.

Toumey, J.W., 1929. Initial root habit in American trees and its bearing on regeneration. In: Duggar, B.M. (Ed.), Proceedings of the International Congress of Plant Sciences. George Banta Publishing Company, Menasha, WI, USA.

Tyree, M.T., Ewers, F.W., 1991. The hydraulic architecture of trees and other woody plants. New Phytol. 119, 345–360.

Van der Werf, A., Visser, A.J., Schieving, F., Lambers, H., 1993. Evidence for optimal partitioning of biomass and nitrogen at a range of nitrogen availabilities for a fast- and slow-growing species. Funct. Ecol. 7, 63–74.

Van Valen, L., 1975. Life, death, and energy of a tree. Biotropica 7, 260–269.

Van Valen, L., 1977. The red queen. Am. Nat. 111, 809–810.

Wagner, G.P., Altenberg, L., 1996. Complex adaptations and the evolution of evolvability. Evolution 50, 967–976.

Weiner, J., 2004. Allocation, plasticity and allometry in plants. Perspect. Plant Ecol. Evol. Syst. 6, 207–215.

Wells, C.E., Eissenstat, D.M., 2001. Marked differences in survivorship among apple roots of different diameters. Ecology 82, 882–892.

Wells, C.E., Glenn, M.D., Eissenstat, D.M., 2002. Changes in the risk of fine-root mortality with age: a case study in peach, *Prunus persica* (Rosaceae). Am. J. Bot. 89, 79–87.

Westoby, M., 1984. The self-thinning rule. Adv. Ecol. Res. 14, 167–225.

Westoby, M., Falster, D.S., Moles, A.T., Vesk, P.A., Wright, I.J., 2002. Plant ecological strategies: some leading dimensions of variation between species. Annu. Rev. Ecol. Syst. 33, 125–159.

White, J., 1981. The allometric interpretation of the self-thinning rule. J. Theor. Biol. 89, 475–500.

Willis, K.J., McElwain, J.C., 2002. The Evolution of Plants. Oxford University Press, New York.

Wood, C.J., 1995. Understanding wind forces on trees. In: Coutts, M.P., Grace, J. (Eds.), Wind and Trees. Cambridge University Press, Cambridge, UK, pp. 133–164.

Wright, I.J., Reich, P.B., Westoby, M., 2001. Strategy shifts in leaf physiology, structure and nutrient content between species of high- and low-rainfall and high- and low-nutrient habitats. Funct. Ecol. 15, 423–434.

Wright, I.J., Reich, P.B., Westoby, M., Ackerly, D.D., Baruch, Z., Bongers, F., Cavender-Bares, J., Chapin, T., Cornelissen, J.H.C., Diemer, M., Flexas, J., Garnier, E., Groom, P.K., Gulias, J., Hikosaka, K., Lamont, B.B., Lee, T., Lee, W., Lusk, C., Midgley, J.J., Navas, M.-L., Niinemets, Ü., Oleksyn, J., Osada, N., Poorter, H., Poot, P., Prior, L., Pyankov, V.I., Roumet, C., Thomas, S.C., Tjoelker, M.G., Veneklaas, E.J., Villar, R., 2004. The worldwide leaf economics spectrum. Nature 428, 821–827.

Wright, I.J., Westoby, M., 2002. Leaves at low versus high rainfall: coordination of structure, lifespan and physiology. New Phytol. 155, 403–416.

Wright, I.J., Westoby, M., Reich, P.B., 2002. Convergence towards higher leaf mass per area in dry and nutrient-poor habitats has different consequences for leaf life span. J. Ecol. 90, 534–543.

Young, J.A., Young, C.G., 1992. Seeds of Woody Plants in North America. Timber Press Inc., Portland, OR, USA.

Zavala, M.A., 2004. Integration of drought tolerance mechanisms in Mediterranean sclerophylls: a functional interpretation of leaf gas exchange simulators. Ecol. Model. 176, 211–226.